



Citation for published version:

Ke, X & Duan, Y 2019, 'A spatially-varying relaxation parameter Lattice Boltzmann Method (SVRP-LBM) for predicting the effective thermal conductivity of composite material', *Computational Materials Science*, vol. 169, 109080. <https://doi.org/10.1016/j.commatsci.2019.109080>

DOI:

[10.1016/j.commatsci.2019.109080](https://doi.org/10.1016/j.commatsci.2019.109080)

Publication date:

2019

Document Version

Peer reviewed version

[Link to publication](#)

Publisher Rights

CC BY-NC-ND

University of Bath

General rights

Copyright and moral rights for the publications made accessible in the public portal are retained by the authors and/or other copyright owners and it is a condition of accessing publications that users recognise and abide by the legal requirements associated with these rights.

Take down policy

If you believe that this document breaches copyright please contact us providing details, and we will remove access to the work immediately and investigate your claim.

Citation:

Ke, X.; Duan, Y., A spatially-varying relaxation parameter Lattice Boltzmann Method (SVRP-LBM) for predicting the effective thermal conductivity of composite material. 2019, 169, 109080. <https://doi.org/10.1016/j.commatsci.2019.109080>

1 A spatially-varying relaxation parameter Lattice Boltzmann
2 Method (SVRP-LBM) for predicting the effective thermal
3 conductivity of composite material

4 Xinyuan Ke^{1*} Yu Duan²

5 1. Department of Architecture and Civil Engineering, University of Bath, Bath BA2
6 7AY, United Kingdom

7 2. Department of Mechanical Engineering, Imperial College London, London, UK

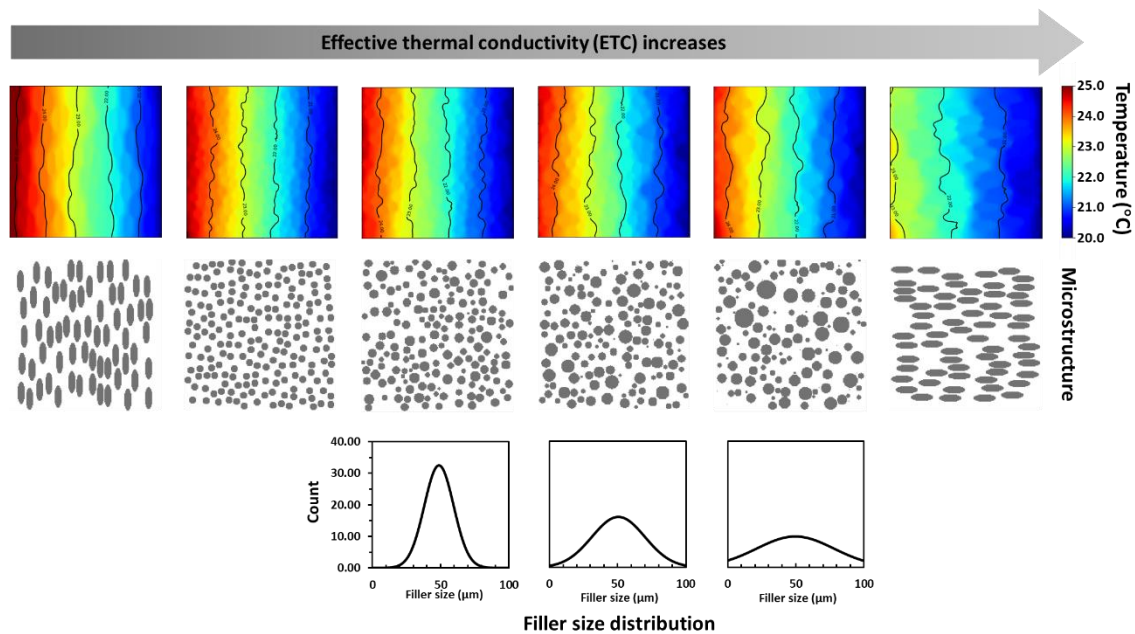
8 *Corresponding author. E-mail: x.ke@bath.ac.uk, Tel: +44 (0) 1225 384020

9 **Highlights**

- 10 - An in-house coded SVRT-LBM solver for predicting effective thermal
11 conductivity
12 - An optimized method to choose spatially varying relaxation parameters
13 - Taking into consideration contact resistance, filler geometry and size
14 distribution

15

16 **Graphic abstract**



17

18 A SVRP-LBM solver for predicting the effective thermal conductivities of composite
19 materials with varying fillers size distributions and geometries.

20

21 **Abstract**

Citation:

Ke, X.; Duan, Y., A spatially-varying relaxation parameter Lattice Boltzmann Method (SVRP-LBM) for predicting the effective thermal conductivity of composite material. 2019, 169, 109080.
<https://doi.org/10.1016/j.commat.2019.109080>

22 Functional filler-reinforced composite materials play critical roles in thermal
23 management in various engineering applications. In this study, an in-house coded
24 spatially-varying relaxation parameter Lattice Boltzmann Method (SVRP-LBM)
25 solver has been developed for predicting the effective thermal conductivity (ETC) of
26 simulated composite materials. A randomly dispersed filler generator (RDFG)
27 incorporating Monte Carlo random sampling method has been developed for
28 reconstructing the microstructure of composite materials. The artificial composite
29 materials with functional fillers of different geometries and particle size are studied.
30 The SVRP-LBM is validated against FVM predictions and theoretical models. The
31 spatially-varying relaxation parameters method has been used to reflect materials with
32 different thermophysical properties, including the interfacial contact resistance
33 between the matrix-filler interfaces. It is demonstrated that the lowest relaxation
34 parameters should be around 1.0 in order to achieve a higher accuracy of LBM
35 predictions. The effects of filler geometry and particle sizes on the ETC are also
36 assessed. The shape and orientation of the anisotropic filler have strong effects on the
37 ETC. After the geometry of the filler in the numerical models being adjusted
38 accordingly to the real fillers, the predictions show good agreement with experimental
39 data. All in all, the SVRP-LBM solver has shown good capability and accuracy for
40 predicting the ETC of composite material.

41 *Keywords:*

42 Lattice Boltzmann
43 Spatially-varying relaxation parameters
44 Numerical prediction
45 Composite materials
46 Effective thermal conductivity
47

48

49

50

51

52

53

54

55

56

57

Citation:

Ke, X.; Duan, Y., A spatially-varying relaxation parameter Lattice Boltzmann Method (SVRP-LBM) for predicting the effective thermal conductivity of composite material. 2019, 169, 109080.
<https://doi.org/10.1016/j.commatsci.2019.109080>

58 **Nomenclature****Letters**

c_s	Pseudo sound speed (m/s)
\vec{c}_i	Discrete lattice speed at direction i (m/s)
d	Dimensionless LBM diffusion coefficient
f_i	Distribution function
f_i^{eq}	Equilibrium distribution function
i	D2Q9 LBM velocity direction ($i=0\sim 8$)
k	Thermal conductivity (W/m·K)
k_{eff}	Effective thermal conductivity (W/m·K)
q	Heat flux (W/m ²)
\vec{r}	Position vector (m)
t	Time (s)
t_{LBM}	Dimensionless LBM time step
w_i	Weighting factor at direction i
A	Composite cross-sectional area (m ²)
C_p	Specific thermal capacity (J/kg·K)
D_{diff}	Thermal diffusivity (m ² /s)
L	Composite thickness (m)
N	Total number of lattice
T	Temperature (K)
ΔT	Temperature difference (K)

Greek symbols

ρ	Density (kg/m ³)
τ	Dimensionless relaxation time
ξ	Average particle size (mean value)
σ^2	Variance
φ	Filler volume fraction
φ_n	Volume fraction of phase n ($n=1, 2, 3 \dots$)
ω	Dimensionless relaxation parameter
Ω_i	Collision operator at direction i

59

60

61

Citation:

Ke, X.; Duan, Y., A spatially-varying relaxation parameter Lattice Boltzmann Method (SVRP-LBM) for predicting the effective thermal conductivity of composite material. 2019, 169, 109080.
<https://doi.org/10.1016/j.commat.2019.109080>

62 1 Introduction

63 In recent decades, there has been rapid progress in the synthesis and processing of
64 composite materials enhanced with functional fillers [1-3]. These functional filler-
65 reinforced composite materials are widely used for thermal management in various
66 applications, such as energy storage [4], electrolyte fuel cell [5], small electronic
67 devices [6, 7], and thermal insulation in buildings [8]. As these materials play more
68 and more important roles in our everyday life, there have been increasing demands for
69 better scientific understanding of the heat transfer process within these materials at
70 microscopic and mesoscopic scales [9].

71 Thermal conduction is the main heat transfer mechanism that occurs in composite
72 materials [10, 11]. The thermal conductivity of composite material plays critical roles
73 in assessing its thermal performances, such as thermal insulation and heat dissipation
74 [11-13]. The effective thermal conductivity (ETC) is the most commonly used
75 parameter for characterising the thermal performance of composite materials [11, 14].
76 The ETC of a composite material is determined by many factors, including the
77 thermophysical properties of both the matrix and filler materials, volume fractions,
78 geometries and distributions of the functional fillers [10, 13, 15]. Both experimental
79 methods and modelling methods can be used to assess the ETC values. The
80 experimental methods include steady-state methods, such as guarded hot plate method,
81 axial flow method, and heat flow meter method; and transient methods, such as flash
82 method, transient hot-wire method, and transient plane source method [16]. The
83 modelling methods include theoretical modelling and numerical modelling. The
84 theoretical models for composite materials can be categorized into two classes, the
85 effective medium approximation (EMA) and the micromechanics method. The EMA
86 methods include the Maxwell-Eucken model [17] and its extensions, while the
87 micromechanics method includes Mori–Tanaka (M-T) model [18] and Benvensite’s
88 model [17]. A summary of these existing theoretical models for predicting ETC of
89 polymer-based composite material can be found in Zhai et al. [14].

90 Owing to the recent development of computational techniques, numerical
91 simulation methods have attracted growing attention as powerful tools to predict the
92 ETC of composite materials at multiple scales [14]. The finite-difference methods
93 (FDM) and finite volume method (FVM) are widely used for the macroscale (>1mm)
94 thermal performance modelling [19, 20]. In comparison, the Lattice Boltzmann
95 Method (LBM) shows better precision and faster time evolution when dealing with
96 heat transfer at mesoscales (1 μ m to 1mm) [21-23]. However, when the nanomaterials
97 (1nm to 1 μ m) are used as functional fillers, such as 2D graphene sheets, molecular
98 dynamic (MD) models are often used to reconstruct their nanoscale features [24]. For
99 functional composite materials, the scales of the fillers, such as metals [1, 25],
100 functional ceramics [6, 7], and graphite [2, 26], are normally around few micrometres,
101 making the LBM a better method to simulate the thermal performance of these
102 materials.

Citation:

Ke, X.; Duan, Y., A spatially-varying relaxation parameter Lattice Boltzmann Method (SVRP-LBM) for predicting the effective thermal conductivity of composite material. 2019, 169, 109080.
<https://doi.org/10.1016/j.commatsci.2019.109080>

103 The Lattice Boltzmann Method (LBM), originated from the lattice gas automata
104 (LGA) method and developed based on the Boltzmann kinetic equation is a powerful
105 mesoscopic approach. The method can cooperate with the complex geometry
106 boundary conditions and various interactions between particles [14, 21]. Wang et al.
107 [27] used LBM to predict the ETC of a random open foam porous material. Lu et al.
108 [28] studied the conjugate heat transfer phenomena at the solid-liquid interfaces using
109 LBM. Fang et al. [29] used LBM to predict the thermal conductivity of braided fabric
110 composites. And, Li et al. [7] used the same method to study the effects of fillers size
111 on the ETC of thermal interfacial material for the heat dissipation in LED.

112 Despite the recent progress in using LBM to predict the ETC of composite
113 materials, tuning of relaxation parameters in order to achieve stable and accurate
114 simulations remains as a challenge [30]. In general, the choice of suitable relaxation
115 parameter (ω) is crucial for the accuracy and stableness of the LBM simulation [23,
116 30]. Wang et al. [31] suggested that the ω should be between 0.5 to 2 to ensure
117 stableness for the simulation of the conjugate heat transfer at the solid-liquid
118 interfaces. Walther et al. [23] suggested that for the ionic diffusion process in two-
119 phase materials with large diffusivity ratios, stable LBM simulation results can only
120 be achieved when the ω for both materials is within 0.1 and 1.0. However, the effect
121 of ω values on simulation accuracy has not yet been discussed.

122 The Monte Carlo random sampling method has been applied for generating of
123 microstructures which is representative of laboratory synthesised materials [22, 32].
124 Zhou et al. [22] used randomly dispersed fillers with uniformly distributed filler sizes.
125 This treatment has its limitation to represent the actual microstructure of composite
126 materials, as particle distributions similar to the normal distribution were often
127 observed in experiments [6]. Deng et al. [33] used statistical self-similarity fractal
128 geometry to reconstruct the self-similar random porous structure; however, the fixed
129 filler location was adapted which was not ideal to represent the composite materials
130 reinforced by randomly dispersed fillers. It remains unclear how the distribution of
131 particle sizes will affect the thermal performance of a composite. The shape of the
132 particles impacts the macroscale thermal properties of the composite material, and
133 should not be neglected [10]. Moreover, the effects of the orientation of fillers need to
134 be better understood, if the filler particles possess the anisotropic shape. In addition,
135 the heat conduction occurred at the interfaces between the functional filler and the
136 matrix material also plays critical roles in the overall thermal performance of the
137 composite material [34-36]. The main physical phenomenon to consider here is
138 interfacial contact resistance due to imperfect contact (or roughness) between the
139 surfaces that leads to large phonon scattering and temperature differences [37]. It
140 would be necessary to test the ability of the LBM solver to reflect this physical
141 phenomenon.

142 In this study, an in-house coded spatially-varying relaxation parameter Lattice
143 Boltzmann Method (SVRP-LBM) solver has been developed for predicting the ETC
144 of various composite materials. The paper is organised as follows: a brief introduction

Citation:

Ke, X.; Duan, Y., A spatially-varying relaxation parameter Lattice Boltzmann Method (SVRP-LBM) for predicting the effective thermal conductivity of composite material. 2019, 169, 109080. <https://doi.org/10.1016/j.commatsci.2019.109080>

145 to the LBM method and randomly dispersed filler generator are included in section 2.
146 Section 3 is contributed to discuss the benchmark study as well as the effect of the
147 spatially varying relaxation parameters on the stableness and accuracy of the LBM
148 simulation. In section 4, the effect of the random features of the fillers, distribution of
149 filler size and location and orientation of the anisotropic fillers, the thermal
150 conduction behaviours between the filler and matrix interfaces are discussed, as well
151 as validation of the SVRP-LBM solver with respect to the real composite materials.

152

153 **2 Methodologies**

154 2.1 Governing equations

155 The heat conduction in the lattice domain is governed by equation (1),

$$\rho C_p \frac{\partial T}{\partial t} = k \nabla^2 T \tag{1}$$

156 where ρ , C_p and k are the density, specific thermal capacity, and thermal conductivity
157 of the material, respectively.

158 2.2. Lattice Boltzmann method

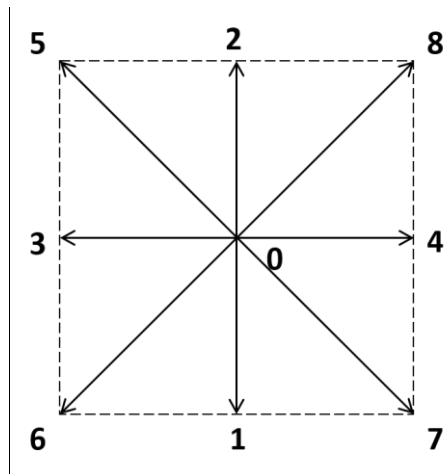
159 In this paper, the single-relaxation-time D2Q9 LBM is used. We will give a brief
160 introduction to the methodology in this section. For readers' interested in this method,
161 please refer to [30, 38] for more information.

162 The kinetic LB equation can be written as,

$$\frac{\partial f_i(\vec{r}, t)}{\partial t} + \vec{c}_i \cdot \frac{\partial f_i(\vec{r}, t)}{\partial \vec{r}} = \Omega_i \tag{2}$$

163 where $f_i(\vec{r}, t)$ represents the probability distribution function in direction i ($i=0\sim 8$,
164 Figure 1) at location \vec{r} at time t . Ω_i is the collision operator.

165



166

167 Figure 1 Schematic diagram of D2Q9 velocity directions model.

Citation:

Ke, X.; Duan, Y., A spatially-varying relaxation parameter Lattice Boltzmann Method (SVRP-LBM) for predicting the effective thermal conductivity of composite material. 2019, 169, 109080.
<https://doi.org/10.1016/j.commatsci.2019.109080>

168

169 In this study, the Bhatnagar-Gross-Krook (BGK) collision approximation is used,
 170 which can be written as [39],

$$\Omega_i = -\frac{1}{\tau} [f_i(\vec{r}, t) - f_i^{eq}(\vec{r}, t)] \quad (3)$$

$$\Delta \vec{r} = \Delta t \cdot \vec{c}_i \quad (4)$$

171 where f_i^{eq} is the equilibrium distribution function and τ is the relaxation time. \vec{c}_i is
 172 the lattice speed at direction i .

173 The discretization of equation (2) to (4) can be written as following,

$$f_i(\vec{r} + \Delta t \cdot \vec{c}_i, t + \Delta t) - f_i(\vec{r}, t) = -\omega \cdot [f_i(\vec{r}, t) - f_i^{eq}(\vec{r}, t)] \quad (5)$$

$$\omega = \frac{\Delta t}{\tau} \quad (6)$$

174 where ω is the relaxation parameter.

175 The bulk properties of density and temperature are obtained by equation (7),

$$T(\vec{r}, t) = \sum_0^8 f_i(\vec{r}, t) \quad (7)$$

176 where T represents the macroscopic temperature.

177 The macroscopic temperature distribution correlates with the mesoscopic
 178 equilibrium distribution function via equation (8) and (9),

$$f_i^{eq} = w_i \cdot T(\vec{r}, t) \quad (8)$$

$$w_i = \begin{cases} \frac{4}{9} & i = 0 \\ \frac{1}{9} & i = 1 \sim 4 \\ \frac{1}{36} & i = 5 \sim 8 \end{cases} \quad (9)$$

179 where w_i is the weighting factor for direction i (Figure 1).

180 The discrete lattice velocity \vec{c}_i is defined as,

$$\vec{c}_i = \begin{cases} 0 & i = 0 \\ (\cos\theta_i, \sin\theta_i) \cdot c_s, & \theta_i = (i-1)\frac{\pi}{2} \quad i = 1 \sim 4 \\ \sqrt{2}(\cos\theta_i, \sin\theta_i) \cdot c_s, & \theta_i = (i-5)\frac{\pi}{2} + \frac{\pi}{4} \quad i = 5 \sim 8 \end{cases} \quad (10)$$

181 where c_s is the pseudo sound speed.

182 According to the Chapman-Enskog Expansion [38], the relaxation parameter ω is
 183 related to the thermal conductivity and thermal diffusivity (D_{diff}) of the material via
 184 equations (11) and (12),

Citation:

Ke, X.; Duan, Y., A spatially-varying relaxation parameter Lattice Boltzmann Method (SVRP-LBM) for predicting the effective thermal conductivity of composite material. 2019, 169, 109080.
<https://doi.org/10.1016/j.commatsci.2019.109080>

$$\frac{k}{\rho C_p} = \frac{c_s^2 \cdot \Delta t}{2} \left(\frac{1}{\omega} - \frac{1}{2} \right) \quad (11)$$

$$D_{diff} = \frac{k}{\rho C_p} \quad (12)$$

185 where $0 < \omega < 2$.

186 In this study, spatially varying relaxation parameters (SVRP) are used to reflect the
 187 heterogeneous thermophysical properties of composite materials at mesoscale [31].
 188 For composite materials composed of two materials, their thermophysical properties
 189 are related to the relaxation parameters as:

$$\frac{D_1}{D_2} = \frac{k_1}{k_2} \times \frac{(\rho C_p)_2}{(\rho C_p)_1} = \frac{\left(\frac{1}{\omega_1} - \frac{1}{2}\right)}{\left(\frac{1}{\omega_2} - \frac{1}{2}\right)} \quad (13)$$

190

191 After the system reaches its equilibrium final state, the effective thermal
 192 conductivity (ETC) is then calculated using equation (14),

$$k_{eff} = \frac{L \cdot \int q \cdot dA}{\Delta T \cdot \int dA} \quad (14)$$

193 where q is the steady state heat flux, ΔT is the temperature difference along the heat
 194 flux direction over a distance of L , and A is the cross-sectional area.

195 2.2 Boundary conditions

196 The insulated boundaries are treated as adiabatic. The isothermal boundary
 197 condition follows the Zou and He bounce-back rule [40], which can be expressed as:

$$f_\alpha - f_\alpha^{eq} = -(f_\beta - f_\beta^{eq}) \quad (15)$$

198 where α and β represent the two opposite directions.

199 Equation (16) is used to approximate the heat flux at the constant heat flux
 200 boundary condition.

$$q' = -k_{phase} \cdot \frac{\partial T}{\partial \vec{r}} \quad (16)$$

201

202 2.3 Randomly dispersed filler generator (RDFG)

203 In this study, a randomly dispersed filler generator (RDFG) has been developed to
 204 mimic microstructures of artificial composite materials. In the RDFG, the scale of the
 205 fillers are governed by the normal distribution $f(x|\mu, \sigma^2)$, which expressed by
 206 equation (17). Meanwhile, the location of the fillers in the domain follows the
 207 uniform distribution. Overlapping of the located fillers is not allowed in this practice.
 208 The contact between the fillers (sharing of the same node) is only allowed when the
 209 total filler fraction is higher than 0.3.

Citation:

Ke, X.; Duan, Y., A spatially-varying relaxation parameter Lattice Boltzmann Method (SVRP-LBM) for predicting the effective thermal conductivity of composite material. 2019, 169, 109080. <https://doi.org/10.1016/j.commatsci.2019.109080>

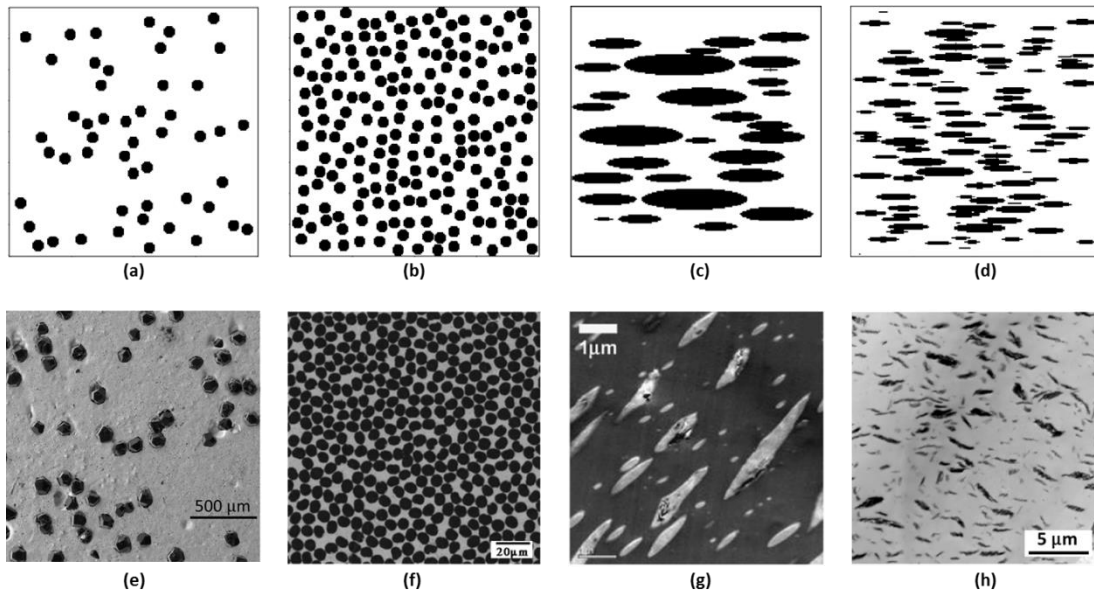
$$f(x|\xi, \sigma^2) = \frac{1}{\sqrt{2\pi\sigma^2}} e^{-\frac{(x-\xi)^2}{2\sigma^2}} \quad (17)$$

210 where ξ is the average particle size and σ^2 is the variance,

211 For the RDFG developed in this study, the average particle size and variance are
212 provided by the users as initial inputs, as well as the total filler volume fraction. For
213 any given number of total fillers, the scalers following the normal distribution as
214 shown in equation (17) will be generated, randomly allocated to the lattice domain
215 and output as black (filler) and white (matrix) images. The total filler volume fraction
216 will be calculated by counting the percentage of black pixels in the entire lattice
217 domain. To achieve a designated total volume fraction, an initial filler number is
218 estimated using the average particle size provided by the user, which will be adjusted
219 stepwise until reaching the designated total filler volume. Since the least
220 increment/decrement possible is depending on the smallest fillers generated following
221 the normal distribution, a deviation below 1.0 % is considered acceptable by the
222 RDFG.

223 Figure 2 gives a view of four simulated artificial composite materials
224 microstructure generated using RDFG with different input parameters, according to
225 the scanning electron microscopy (SEM), or transmission electron microscopy (TEM)
226 images reported in the literature [41-44]. Figure 3 and Figure 4 show examples of
227 simulated microstructure of composite material consist of fillers (spherical or
228 elliptical) with varying sizes. And, sizes of the particles in each composite follow the
229 normal distribution.

230
231



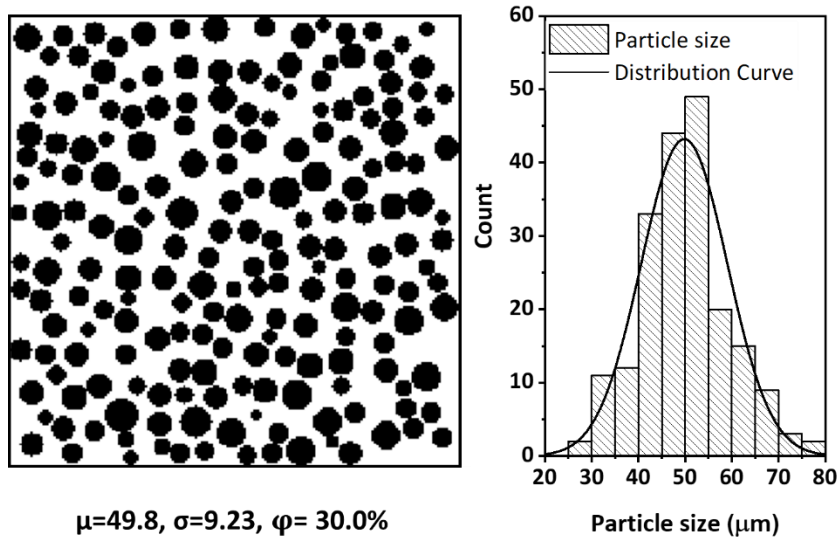
232

233 Figure 2 (a) to (d), schematics of the generated composite material microstructure
234 with fillers of different sizes, geometries and volume fractions using the described

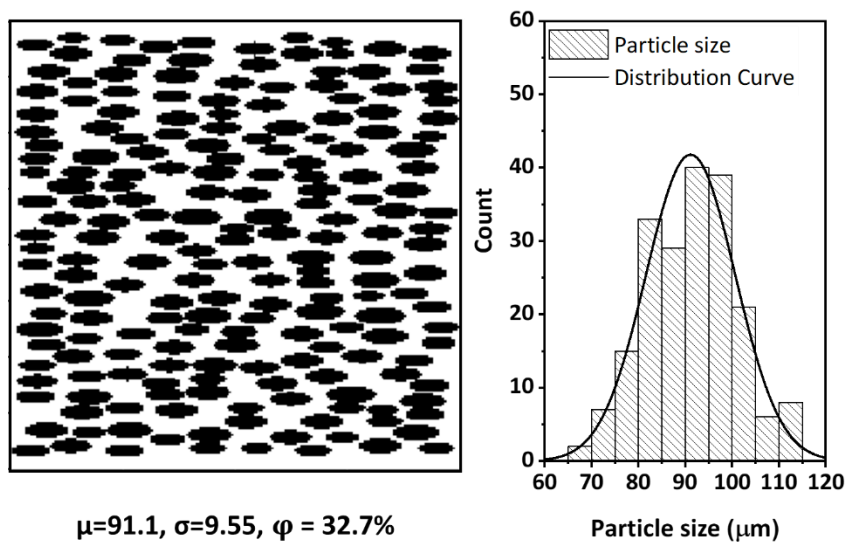
Citation:

Ke, X.; Duan, Y., A spatially-varying relaxation parameter Lattice Boltzmann Method (SVRP-LBM) for predicting the effective thermal conductivity of composite material. 2019, 169, 109080. <https://doi.org/10.1016/j.commatsci.2019.109080>

235 RDFG computational method (200x200), and comparison with the microstructure of
236 real composite materials. (e) SEM image of Cu/D composite, adapted from [41] with
237 permission from Elsevier; (f) BSE image of carbon fibre reinforced bulk metallic
238 glass composite, reproduced from [42], with the permission of AIP Publishing; (g)
239 TEM image of a typical PC/PBT/Talc composite, adapted from [43] with permission
240 from Elsevier; (h) TEM image of PLA/talc composite, adapted from [44] with
241 permission from John Wiley and Sons;



243 Figure 3 Schematic diagram of the microstructure with spherical fillers of normally
244 distributed particle sizes.



246 Figure 4 Schematic diagram of the microstructure with elliptical fillers of normally
247 distributed particle sizes. The values of semi-major axis of the ellipses were used for
248 plotting the particle size distribution.

249

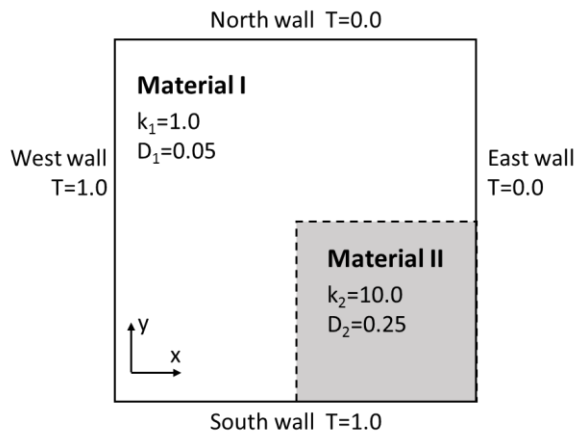
Citation:

Ke, X.; Duan, Y., A spatially-varying relaxation parameter Lattice Boltzmann Method (SVRP-LBM) for predicting the effective thermal conductivity of composite material. 2019, 169, 109080.
<https://doi.org/10.1016/j.commatsci.2019.109080>

250 3 Benchmark Studies

251 3.1 Comparison with the finite volume method

252 Before applying the in-house developed LBM in the further application, the code is
 253 first validated against a simulation based on the finite volume method (FVM) in this
 254 section. It is worth to mention that the LBM code and RDFG are developed using
 255 Python 3, while the FVM is a Fortran code. In the FVM code, the heat conduction
 256 equation is discretized using the 2nd order central differencing scheme. Two codes are
 257 applied to simulate the heat conduction via a plate which is made from two materials,
 258 Material I and II. The geometry of the validation case is illustrated in Figure 5. Both
 259 materials possess different thermal conductivities and diffusivities. The dimensionless
 260 conductivity and diffusivity of Material I are $k_1=1.0$ and $D_1=0.05$, respectively, while
 261 these two properties (dimensionless) of Material II are $k_2 =10.0$, $D_2 =0.25$. The
 262 Material II occupies the bottom left quarter, while elsewhere is filled with Material I.
 263 The dimensionless temperature on the west and south wall are set as $T=1$, while the
 264 dimensionless temperature on the other two walls are set as $T=0$.



265

266 Figure 5 Schematic diagram of 2-D problem with dimensionless boundary conditions
 267 and thermophysical properties of different materials. The length along x-axis and y
 268 axis both have been set to 1(dimensionless).

269

270 For the LBM simulation, a lattice domain of 200×200 is used. The relaxation
 271 parameter ω_1 and ω_2 of material I and II are determined according to equation (13).
 272 The ω_1 and ω_2 in the current case are set as 1.67 and 1.00, respectively. In the FVM
 273 simulation, the domain is discretized using the 80×80 mesh. The mesh independent is
 274 achieved in the FVM simulation.

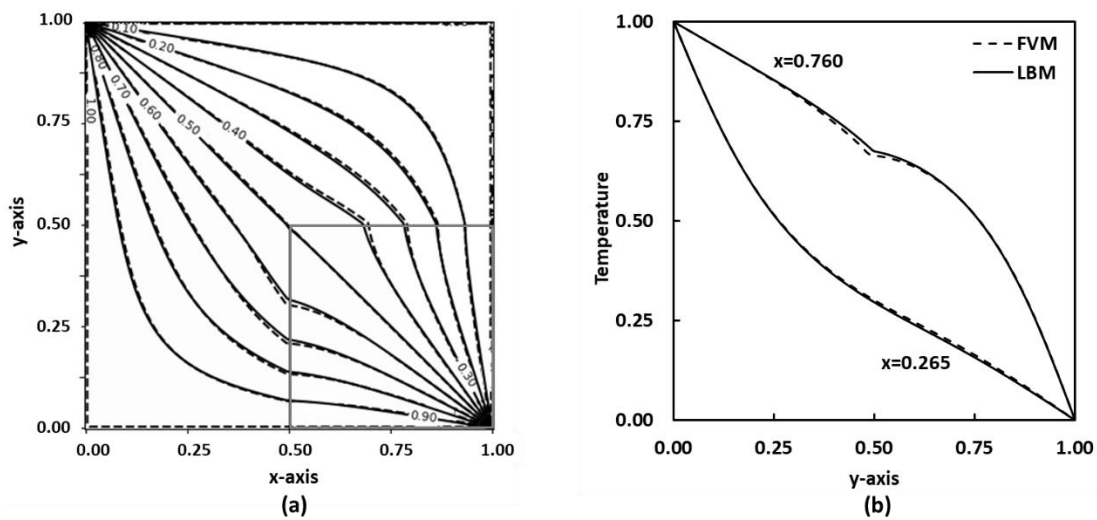
275 The temperature outputs at the equilibrium state of both LBM and FVM
 276 simulations are compared in Figure 6. The temperature contours (Figure 6a) of both
 277 simulations show good agreement between two methods. To exam the results with
 278 more details, the vertical temperature profile at $x = 0.265$ and $x = 0.760$ are compared
 279 in Figure 6b. At $x = 0.265$, where the line crosses only the region of Material I, the

Citation:

Ke, X.; Duan, Y., A spatially-varying relaxation parameter Lattice Boltzmann Method (SVRP-LBM) for predicting the effective thermal conductivity of composite material. 2019, 169, 109080. <https://doi.org/10.1016/j.commatsci.2019.109080>

280 temperature profiles by both methods overlap with each other. At $x = 0.760$, where
281 the line crosses Material I and Material II, there shows an observable difference
282 between the outputs of two methods. However, differences only appear around the
283 interfaces between two materials. This inconsistency lies in the fundamental
284 difference of two methods in the treatment of heat transfer around the interfaces. In
285 the FVM, the heat transfer around the interfaces of two materials is approximated
286 using the information from the cells at both sides of the interface because of the
287 numerical scheme. In the LBM, different relaxation parameters are assigned to the
288 lattice nodes within different materials, and no special treatment at the interfaces is
289 made. But such difference is deemed to be ignorable as suggested in [45].

290



291

292 Figure 6 (a) Comparison between the LBM (solid lines) and FVM (dashed lines)
293 prediction at the equilibrium steady state. (b) Comparison between the LBM (solid
294 lines) and FVM (dashed lines) at $x=0.265$ and $x=0.760$.

295

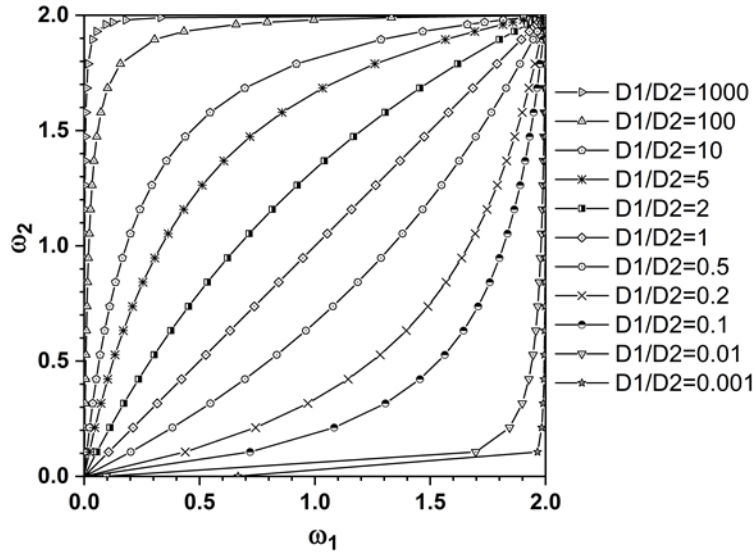
296 3.2 Sensitivity study of relaxation parameters for high diffusivity ratios

297 In this section, the effects of the relaxation parameters on the accuracy and
298 efficiency of the LBM simulation are discussed. As suggested by equation (13), the
299 relaxation parameters ω_1 and ω_2 are related to the diffusivity ratio of two materials
300 (D_1/D_2). Figure 7 shows the correlations between ω_1 and ω_2 when the D_1/D_2 ratio
301 ranges from 0.001 to 1000. As illustrated in the figure, the values of ω_1 and ω_2 are
302 positively correlated for a fixed D_1/D_2 ratio. When $0.01 < D_1/D_2 < 100$, it is easy to
303 set one relaxation parameter to 1 while letting the other relaxation parameter to be
304 slightly above 1 (over-relaxation). In the cases of large diffusivity ratios ($D_1/D_2 >$
305 100 or $D_1/D_2 < 0.01$), one of the relaxation parameters has to be closer to the lower
306 (0.0) or upper limit (2.0) of the allowed value, regardless of the other relaxation
307 parameter, which might cause significant numerical instability [23].

308

Citation:

Ke, X.; Duan, Y., A spatially-varying relaxation parameter Lattice Boltzmann Method (SVRP-LBM) for predicting the effective thermal conductivity of composite material. 2019, 169, 109080. <https://doi.org/10.1016/j.commatsci.2019.109080>



309

310 Figure 7 Relation between ω_1 and ω_2 when the diffusivity ratio D_1/D_2 ranges from
311 0.001 to 1000.

312

313 The LBM time step is related to the real-time scale via equation (18) and (19) [23,
314 38].

$$\frac{t}{t_{LBM}} = \frac{d \times L^2}{D \times N^2} \tag{18}$$

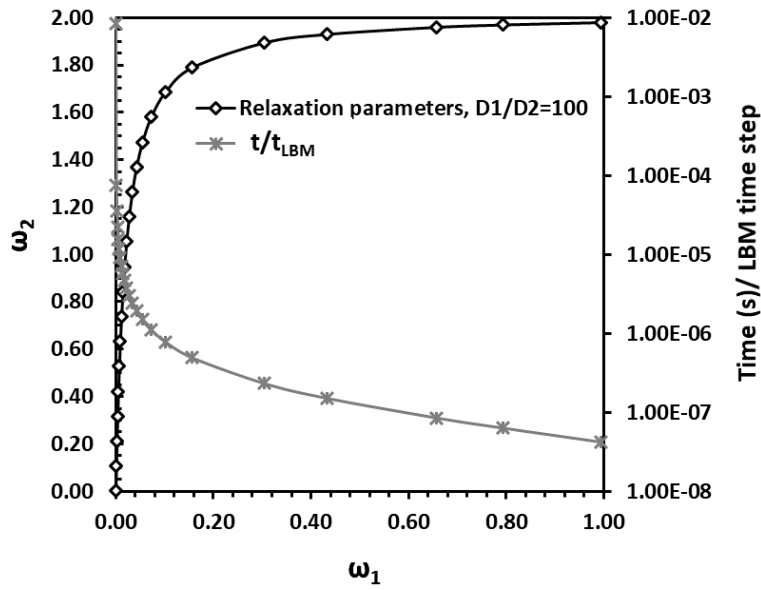
$$d = c_s^2 \left(\frac{1}{\omega} - \frac{1}{2} \right) \tag{19}$$

315 , where t , D and L represent the real-time, diffusion coefficient (m^2/s) and length
316 scale, while t_{LBM} , d and N represent the dimensionless LBM time step, LBM diffusion
317 coefficient and total number of lattice.

318 Figure 8 shows the correlations between the chosen relaxation parameters and the
319 time evolution scale per LBM time step at the diffusivity ratio (D_1/D_2) of 100, whilst
320 N is 200, L is 10^{-3} m, and D_2 is 1.0×10^{-6} m^2/s . As shown in the figure, the time
321 evolution per LBM time step will always decrease as the selected relaxation
322 parameter values increases, while the absolute value of the time evolution per
323 iteration is dependent on the thermal property of the material and the resolution of the
324 lattice.

Citation:

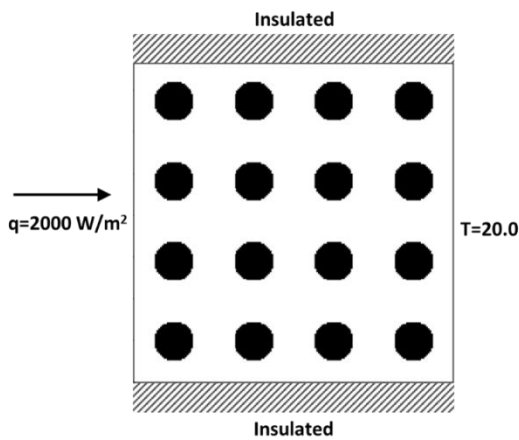
Ke, X.; Duan, Y., A spatially-varying relaxation parameter Lattice Boltzmann Method (SVRP-LBM) for predicting the effective thermal conductivity of composite material. 2019, 169, 109080. <https://doi.org/10.1016/j.commatsci.2019.109080>



325

326 Figure 8 Relation between relaxation parameter ω_1 and ω_2 at the diffusivity ratio
 327 (D_1/D_2) of 100 (black line with diamond markers), and the time evolution per LBM
 328 time step (t/t_{LBM}) under the corresponded chosen relaxation parameter ω_1 and ω_2 (grey
 329 line with star markers).

330



331

332 Figure 9 Schematic diagram of a periodically dispersed spheres model with boundary
 333 conditions

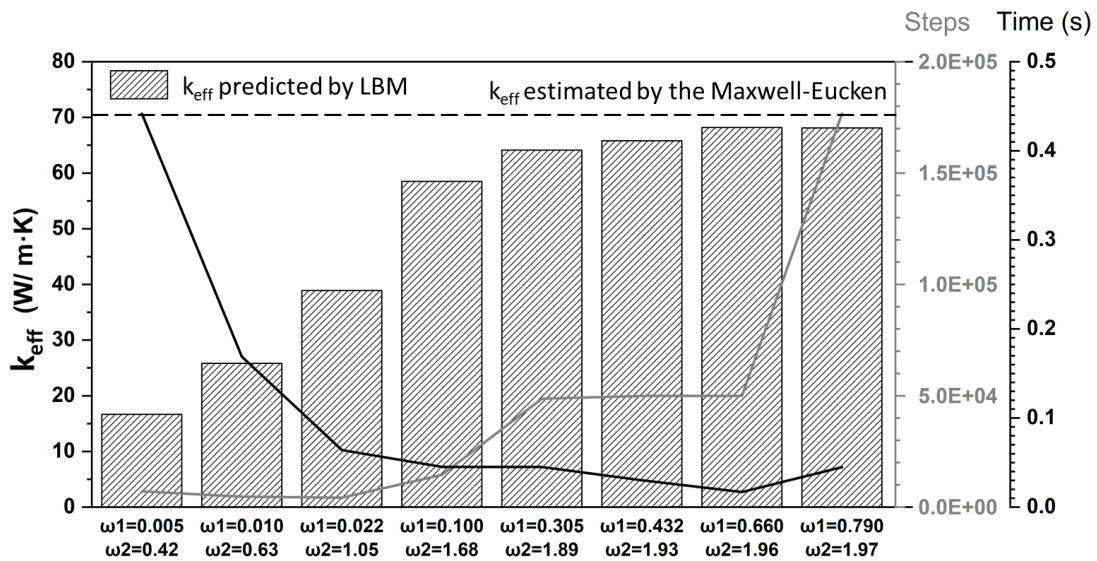
334

335 A case with periodically distributed spherical particles in the lattice domain is
 336 created to investigate the effect of the relaxation parameters on the simulation
 337 accuracy. A view of the geometry can be found in Figure 9. The conductivities of the
 338 spherical fillers and the main matrix are 1 W/m·K and 100 W/m·K, respectively. The
 339 heat flux on the left wall is set as 2000 W/m² and the temperature on the right wall is
 340 fixed at 20.0 °C while the other two walls are treated as adiabatic. The volume
 341 fraction of the fillers shown in Figure 9 is 20.6%.

Citation:

Ke, X.; Duan, Y., A spatially-varying relaxation parameter Lattice Boltzmann Method (SVRP-LBM) for predicting the effective thermal conductivity of composite material. 2019, 169, 109080.
<https://doi.org/10.1016/j.commatsci.2019.109080>

342 Figure 10 compares the predicted ETCs of the simulated composite using different
 343 relaxation parameters for these two materials. The least numbers of LBM time steps
 344 required for each case to reach the equilibrium final states are also plotted in Figure
 345 10, together with the correlated real-time evolution based on the correlation shown in
 346 Figure 8. The predicted ETCs using different relaxation parameters are compared to
 347 the prediction using the Maxwell-Eucken model (equation (22)). More discussions
 348 about the Maxwell-Eucken model will be included in the next section. As the
 349 relaxation parameters increase, the accuracy of the LBM prediction (in comparison
 350 with theoretical values) increases, as well as the number of LBM time steps required
 351 for reaching the equilibrium state. The correlated real-time evolution at initial
 352 equilibrium decreased from 0.110s to 0.004s, as ω_1 increased from 0.005 to 0.660.
 353 However, after ω_1 being increased from 0.660 to 0.790, the ETC remains similar,
 354 while the total number of iteration required for reaching the equilibrium final state
 355 increases by approximately three times. The slight increase in the correlated time
 356 evolution when ω_1 is set to 0.79 is likely due to the nearly tripled LBM time steps
 357 required for the equilibrium state. The result here suggests that for a system with high
 358 diffusivity ratios, when the lower ω value approaches 1, the accuracy of the prediction
 359 increases as well as the LBM time steps required for the equilibrium state. In practical,
 360 a trade-off between prediction accuracy and simulation time needs to be considered.



361

362 Figure 10 Evolution of calculated effective thermal conductivity (k_{eff}) versus LBM
 363 time steps, comparing the use of different relaxation times.

364

365 3.3 Comparison with Maxwell-Eucken model

366 The Maxwell-Eucken model, derived from the effective electric resistivity of a
 367 sphere containing N spherical particles based on the theory of electric potential
 368 satisfying the Laplace equation, is one of the most commonly used effective medium
 369 approximation (EMA) approach for predicting the ETCs of composites [46]. The
 370 Maxwell-Eucken model can be expressed as

Citation:

Ke, X.; Duan, Y., A spatially-varying relaxation parameter Lattice Boltzmann Method (SVRP-LBM) for predicting the effective thermal conductivity of composite material. 2019, 169, 109080. <https://doi.org/10.1016/j.commatsci.2019.109080>

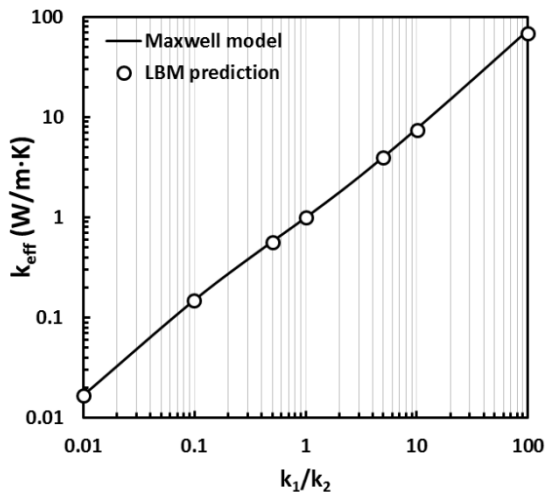
371

$$k_{eff} = k_1 \cdot \frac{2k_1 + k_2 + 2\varphi_2 \cdot (k_2 - k_1)}{2k_1 + k_2 - \varphi_2 \cdot (k_2 - k_1)} \quad (22)$$

372 , where k_1 and k_2 represent the thermal conductivities of the matrix and periodically
373 dispersed spherical fillers, and φ_2 represent the volume fraction of the filler.

374 The Maxwell-Eucken model is particularly effective for predicting the ETC of
375 composite materials reinforced by low volume fraction well-dispersed particles. A
376 view of the simulated case is included in Figure 9. The spherical fillers in the lattice
377 domain distribute periodically and non-interacting. The volume heat capacity (ρC_p) of
378 these artificial materials are set to be unity [21], which means $D_1/D_2 = k_1/k_2$. The
379 thermal conductivity of the matrix is k_1 while the thermal conductivity of the filler is
380 k_2 . Under different k_1/k_2 ratios, k_1 is varying from 0.01 W/m·K to 100 W/m·K, while
381 k_2 is fixed as 1 W/m·K. Hence, the D_1/D_2 ranges from 0.01 to 100. The relaxation
382 parameters chosen for each material are selected according to the observations in
383 section 3.2. More LBM time steps are required for reaching the equilibrium state
384 when the k_1/k_2 becomes much larger (or smaller) than 1. Figure 11 compares the
385 ETCs of artificial composites containing periodically dispersed spheres using LBM
386 and Maxwell-Eucken model under different k_1/k_2 ratios. Well agreement between the
387 theoretical Maxwell-Eucken model prediction and LBM prediction. The deviations
388 between the predictions and the theoretical models are below 2.0%, the accuracy of
389 which is sufficient enough for this application [27, 47]. This proves that the LBM
390 algorithm developed in this study is valid for predicting the ETCs of composite
391 materials reinforced by periodically dispersed spherical fillers under a wide range of
392 k_1/k_2 values.

393



394

395 Figure 11 Predicted effective thermal conductivities of under different k_1/k_2 .

396

Citation:

Ke, X.; Duan, Y., A spatially-varying relaxation parameter Lattice Boltzmann Method (SVRP-LBM) for predicting the effective thermal conductivity of composite material. 2019, 169, 109080.
<https://doi.org/10.1016/j.commatsci.2019.109080>

397 3.4 Comparison with serial and parallel models

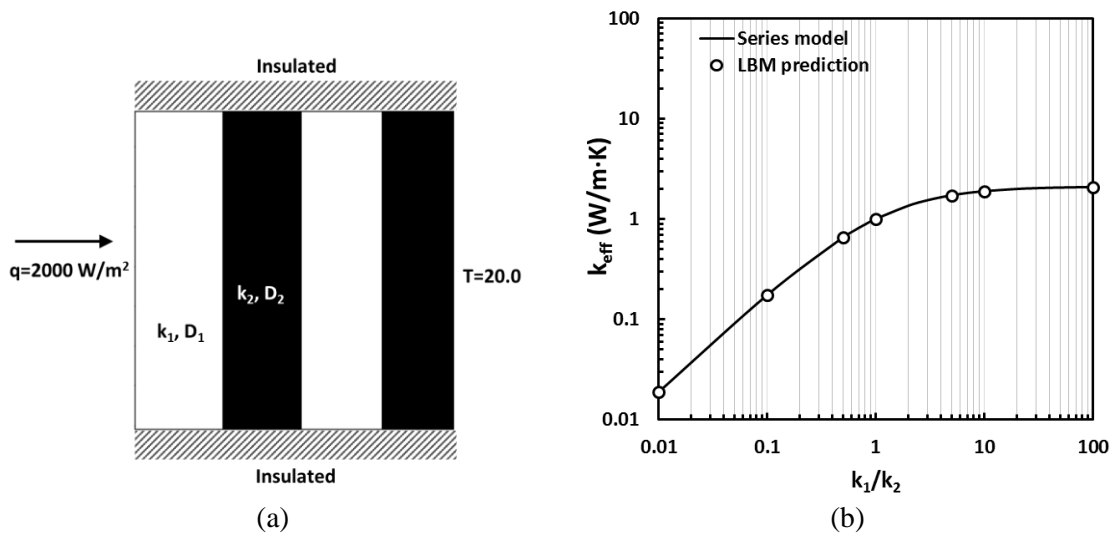
398 Series and parallel models, with the interfaces of two materials either
 399 perpendicular or parallel to the heat flux direction (Figure 12a and c), are proposed to
 400 be used as the simplified representation of the complicated composite material
 401 microstructure [48]. The layers-in-series and the layers-in-parallel models are
 402 simplified representations of the highest and lowest estimated values in a two-phase
 403 composite material [1]. These two models also play very important roles in studying
 404 the interfacial effect between the two materials [28]. The theoretical models for
 405 predicting the ETCs of series and parallel models were derived based on circuit
 406 network of conductors [48], which can be expressed as equation (20) and (21),
 407 respectively.

$$k_{eff} = \frac{k_1 \cdot k_2}{\varphi_2 \cdot k_1 + \varphi_1 \cdot k_2} \quad (20)$$

$$k_{eff} = \varphi_1 \cdot k_1 + \varphi_2 \cdot k_2 \quad (21)$$

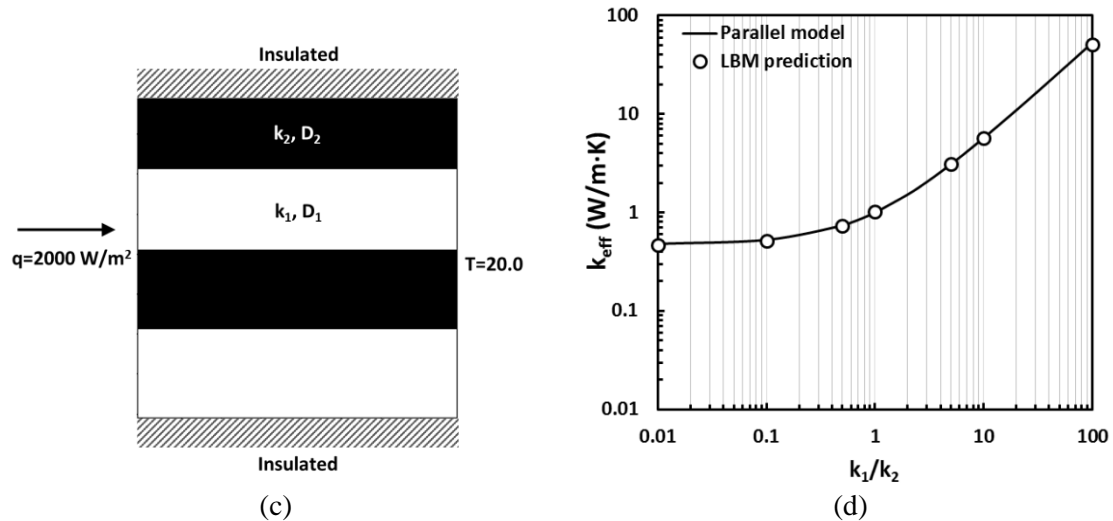
408 , in which φ_1 and φ_2 represent the volume fraction of materials with thermal
 409 conductivity of k_1 and k_2 .

410 Again, ρC_p of these artificial materials are set to be unity [21], and the relaxation
 411 parameters for each material are selected as in the previous section. The k_2 value is
 412 kept at 1.0 while the k_1 value varies from 0.01 to 100. Figure 12 (b) and (d) compares
 413 the predicted ETCs using the LBM solver and the theoretical models. The results by
 414 the LBM solver show good agreement with theoretical values. The deviations
 415 between numerical outputs and theoretical values are within 1.0% for both series and
 416 parallel geometries. This again approves the good capability of this in-house LBM
 417 solver.



Citation:

Ke, X.; Duan, Y., A spatially-varying relaxation parameter Lattice Boltzmann Method (SVRP-LBM) for predicting the effective thermal conductivity of composite material. 2019, 169, 109080.
<https://doi.org/10.1016/j.commatsci.2019.109080>



418 Figure 12 Schematic diagram of (a) periodic series model , and (b) predicted effective
 419 thermal conductivities with different k_1/k_2 ratios; (c) periodic parallel model with
 420 boundary conditions, and (d) predicted effective thermal conductivities with different
 421 k_1/k_2 ratios. The k_2 value is kept as 1 W/m·K in all cases.

422 4 ETC of composite with randomly distributed fillers

423 4.1 Effect of shape and size of artificial representatives

424 The RDFG is used to generate the simulated composite materials reinforced by
 425 randomly dispersed fillers. Firstly, the effects of filler geometry (orientation and
 426 shape) on the thermal conduction of simulated composite materials are discussed
 427 (Figure 13 and Figure 14). Then the effects of filler size variation on the ETC are
 428 studied using spherical fillers following different size distribution (Figure 15).

429 To study the effects of orientations of anisotropic fillers, elliptical fillers with the
 430 aspect ratio of 3:1 and the minor axis value of 50 μm are generated, with their major
 431 axis either perpendicular (Figure 13A) or parallel to the heat flux direction (Figure
 432 13C). These two orientations are chosen to represent the two extreme scenarios of the
 433 elliptical filler geometry in a composite material [49]. For studying the effect of filler
 434 shapes, spherical fillers of diameter 50 μm (Figure 13B) are generated as the
 435 comparison with the elliptical fillers. Spherical fillers of larger diameters, 70 μm
 436 (Figure 13D), are generated to studying the size effect. Three total filler volume
 437 fractions, 6.4%, 13.0% and 26.3%, are considered for each type of filler. In all of
 438 these cases, the thermal conductivity of the matrix materials is 0.2 W/m·K (k_1) and the
 439 thermal conductivity of the fillers (k_2) is 20.0 W/m·K. The volume heat capacities
 440 (ρC_p) of these artificial materials are set to be 1. The heat flux on the left wall ($x=0$) is
 441 2000 W/m² and the temperature on the right wall ($x = 1000 \mu\text{m}$) is 20.0 °C while the
 442 other two walls ($y=0$ and $y=1000 \mu\text{m}$) are treated as adiabatic.

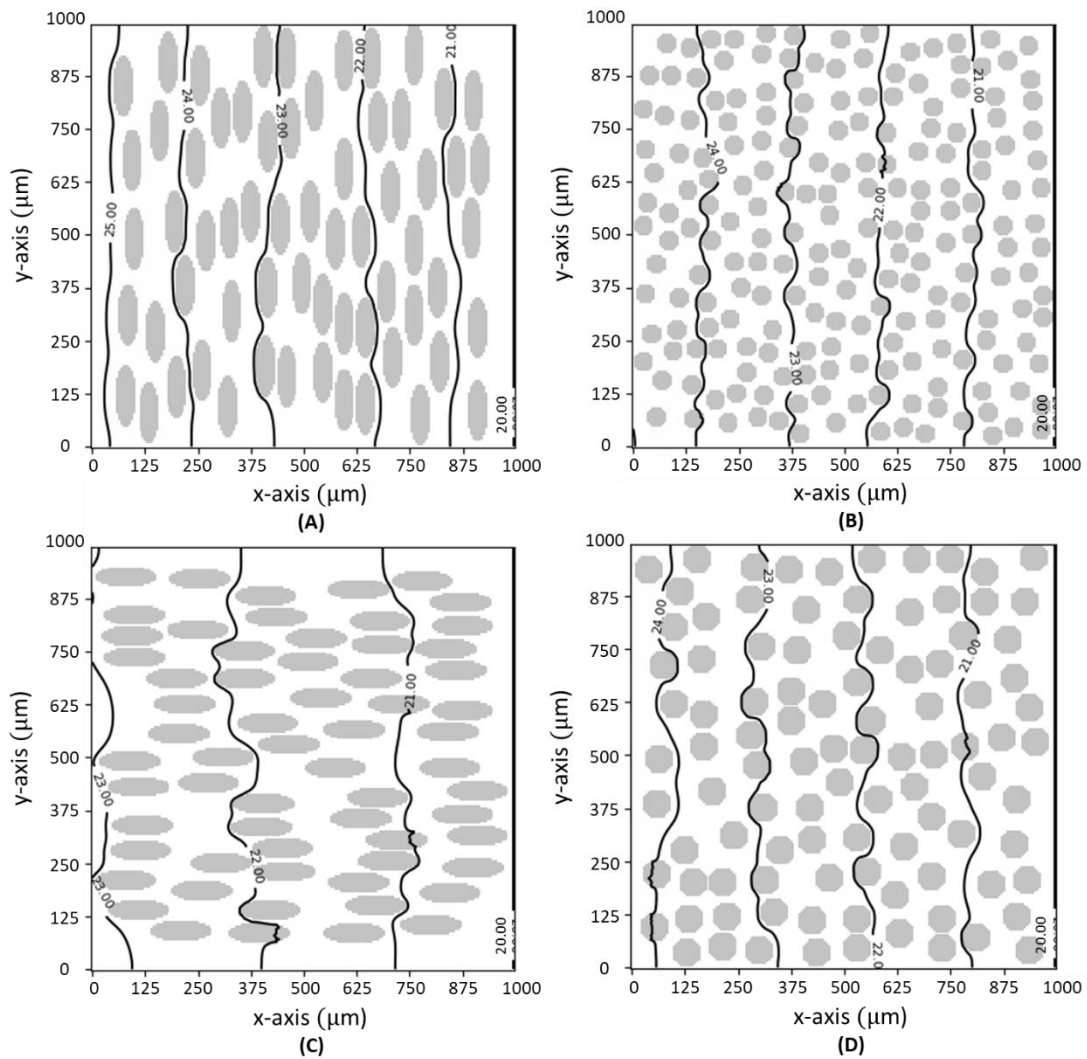
443 The temperature contour plots of these simulated composite materials (with total
 444 volume fraction of $26.3 \pm 0.4\%$) at the equilibrium states are shown in Figure 13. As
 445 expected, the temperature fields are influenced by the conductivities of the local

Citation:

Ke, X.; Duan, Y., A spatially-varying relaxation parameter Lattice Boltzmann Method (SVRP-LBM) for predicting the effective thermal conductivity of composite material. 2019, 169, 109080. <https://doi.org/10.1016/j.commatsci.2019.109080>

446 materials, and the non-uniform microstructure leads to the variation of temperature
447 distribution perpendicular to the heat flux direction. According to the Fourier's law
448 for heat conduction, the local temperature distribution within the sample matrix is
449 positively correlated to the thermal conductivity of the material filled within the
450 location. The local heat transfer would be more efficient (lower temperature gradient)
451 within the highly thermal conductive filler materials than that within the matrix
452 materials. This might explain the correlation between the filler geometry and the
453 temperature distribution within the lattice domain as shown in Figure 13. Based on the
454 temperature contours in the Figure 13, the highest temperature drop across the domain
455 is observed in the case that the elliptical fillers are perpendicular to the heat flux
456 direction (Figure 13A), while the lowest temperature gradient is observed from where
457 the elliptical fillers are parallel to the heat flux direction (Figure 13C). In the case of
458 spherical fillers, seeing Figure 13B and Figure 13D, a higher temperature gradient is
459 shown in the lattice domain reinforced with smaller fillers.

460



461

Citation:

Ke, X.; Duan, Y., A spatially-varying relaxation parameter Lattice Boltzmann Method (SVRP-LBM) for predicting the effective thermal conductivity of composite material. 2019, 169, 109080.
<https://doi.org/10.1016/j.commatsci.2019.109080>

462 Figure 13 Temperature contour plots at the equilibrium final state of simulated
463 composite material reinforced by (A) elliptical fillers vertical to the heat flux direction,
464 (B) spherical fillers with diameter of 50 μm , (C) elliptical fillers parallel to the heat
465 flux direction, and (D) spherical fillers with diameter of 70 μm . The total filler
466 volume fractions in all simulated materials were the same, $26.3 \pm 0.4\%$.

467

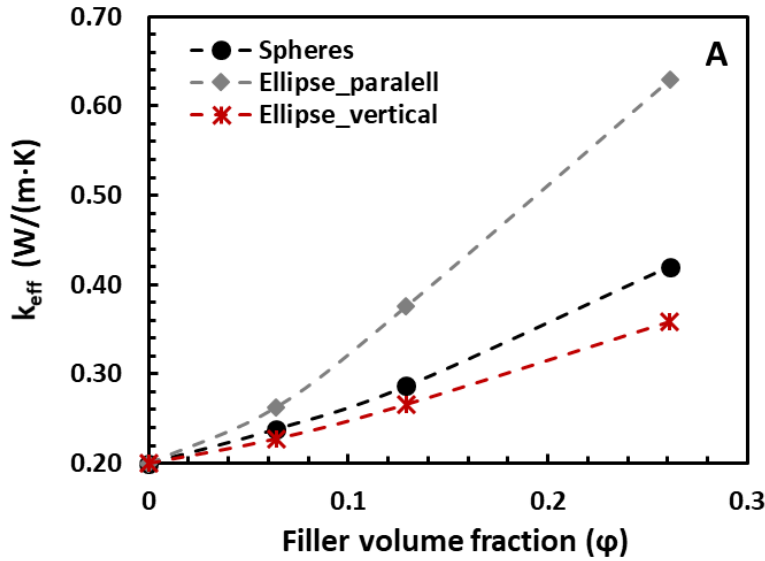
468 The ETCs of simulated composite materials are plotted as a function of filler
469 volume fraction (ϕ) in Figure 14. The ETC values are calculated according to
470 equation (14). The results show that the predicted ETC values always increase as the
471 simulated filler volume fraction increase, same as what normally been observed from
472 polymer composite reinforced by conductive fillers [6, 7, 50]. At the same filler
473 volume fraction, the shape of the filler and its orientation show the dominate effect on
474 the ETC, seeing Figure 14A. For materials reinforced by elliptical fillers with a long
475 axis perpendicular to the heat flux direction, the predicted ETCs are much higher than
476 that reinforced by spherical fillers. The lowest ETC is predicted as the composite is
477 enforced by the elliptical filler with the long axis parallel to the heat flux direction.
478 The differences between predicted ETC values between using elliptical fillers and
479 spherical fillers increase as the filler volume fraction increases. The higher ETC of the
480 composite containing elliptical fillers parallel to the heat flux direction is likely due to
481 the enhanced thermal conductive path along the heat flux direction [16]. When the
482 elliptical fillers are perpendicular to the heat flux, the thermal conductive path is
483 enhanced along the y-axis (the major axis of the filler), however, the ETC is measured
484 along the heat flux direction (x-direction). Since the minor axis of the elliptical filler
485 is set to equal to the diameter of the spherical fillers, therefore at the same filler
486 volume fraction, the filler volume density along the heat flux direction is higher in
487 spherical filler geometry (Figure 13B) than that in the vertical elliptical fillers (Figure
488 13A). This might explain the lower ETC in the vertical elliptical fillers geometries
489 than that in the dispersed spherical filler geometry.

490 Figure 14B compares the effect of filler scale on the ETC. The sphere filler is
491 adopted in this study. The results show that simulated composite materials with larger
492 particle sizes have higher ETC as predicted by LBM. This result is in good agreement
493 with experimental observations [6, 50]. The similar trend was also reported by Zhou
494 et al. [22] and Li et al. [7] using LBM methods, although different interfacial
495 treatments between the filler and the composite matrix are applied in our study. As
496 discussed previously, the efficiency of heat transfer within the sample domain would
497 be slowed down when the heat flux goes from the highly conductive filler to the low
498 conductivity matrix. Comparing with large filler particles, the small particles have
499 higher specific surface area. Therefore, at the same total filler volume fraction, the
500 number of lattice nodes experiencing this “slow down” process would be higher in
501 simulated composite with smaller filler sizes.

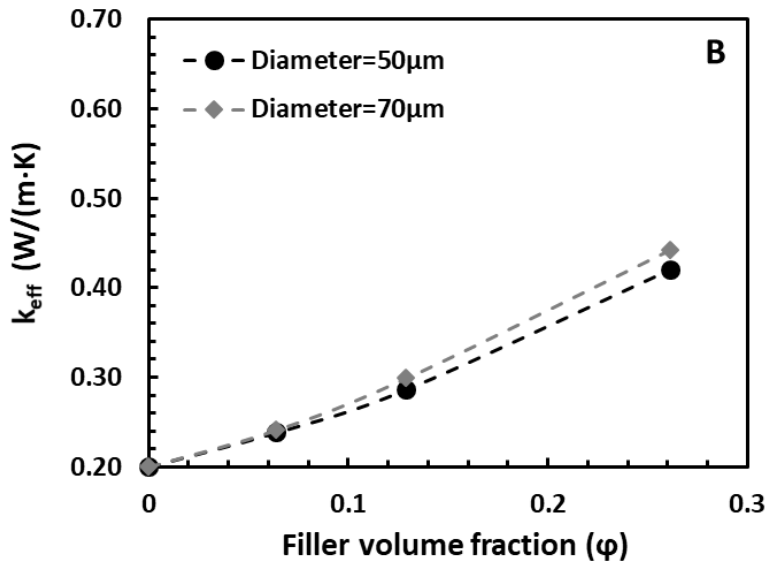
502

Citation:

Ke, X.; Duan, Y., A spatially-varying relaxation parameter Lattice Boltzmann Method (SVRP-LBM) for predicting the effective thermal conductivity of composite material. 2019, 169, 109080. <https://doi.org/10.1016/j.commatsci.2019.109080>



503



504

505 Figure 14 Comparison of effects of A) particle shapes and orientations, B) particle
506 sizes on the predicted effective thermal conductivities using LBM at different filler
507 volume fractions, where $k_1/k_2=0.01$, $k_1=0.2$ W/m·K.

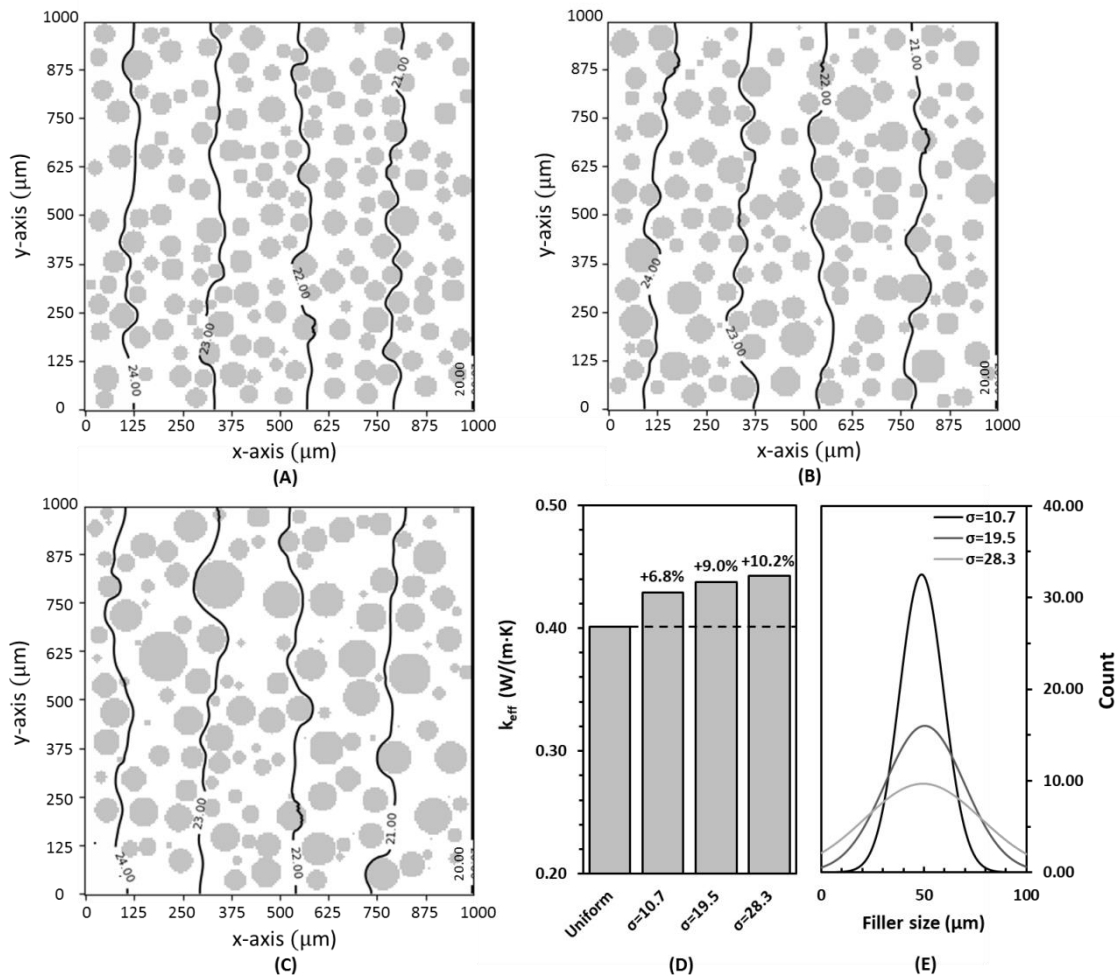
508

509 Although the (diameter) size of the functional fillers is in positive correlation with
510 the thermal conduction efficiency in composite materials containing uni-sized fillers,
511 as suggested in Figure 14B and also supported by experimental observations [6, 50],
512 this positive correlation is nonlinear and controlled by varies factors [51]. One of
513 them is the varying filler size. Figure 15 compares the temperature contours in three
514 composite materials reinforced by spherical fillers with varying sizes. It should be
515 noted that the total filler volume fraction is fixed as $26.3 \pm 0.8\%$. The distribution of
516 the filler size follows the normal distribution, as defined in equation (17). In these
517 three cases, the average filler diameters are the same (50 μ m), but the standard
518 deviations are 10.7 μ m, 19.5 μ m and 28.3 μ m, respectively. Figure 15E shows the

Citation:

Ke, X.; Duan, Y., A spatially-varying relaxation parameter Lattice Boltzmann Method (SVRP-LBM) for predicting the effective thermal conductivity of composite material. 2019, 169, 109080.
<https://doi.org/10.1016/j.commatsci.2019.109080>

519 fitted filler size distribution curve. Similar to that shown in Figure 13, the temperature
 520 field is influenced by the local microstructures, where much significant heterogeneous
 521 temperature distribution can be observed from the materials containing fillers of
 522 larger variance. Figure 15D summaries the predicted ETC of these three
 523 microstructures in comparison with fillers of uniform diameters (50 μm). Although the
 524 average diameters are the same, the filler size variations result in enhancement of
 525 ETC of the matrix. As suggested by Li et al. [7], the filler size effect is particularly
 526 significant on ETC at higher filler volume fraction (>20%). This is because the
 527 composite containing fillers of larger size variation might be able to achieve more
 528 efficient filler packing, thus enhancing the thermal conduction path and improving the
 529 thermal conductivity. This matches with experimental observations where hybrid
 530 fillers can often achieve better enhanced ETC due to the enhanced thermal conduction
 531 path through the sample [50, 52].



532

533 Figure 15 Temperature contour plots at the equilibrium final state of simulated
 534 composite material reinforced by spherical fillers of the different size distribution, (A)
 535 $\sigma=10.7$, (B) $\sigma=19.5$, (C) $\sigma=28.3$. For all these three simulated materials, the mean
 536 filler diameter is 50 μm and the total filler volume fractions are $26.3\pm 0.8\%$. (D) The
 537 predicted ETC values and (E) the fitted filler size distribution curves, for each
 538 simulated microstructure.

Citation:

Ke, X.; Duan, Y., A spatially-varying relaxation parameter Lattice Boltzmann Method (SVRP-LBM) for predicting the effective thermal conductivity of composite material. 2019, 169, 109080. <https://doi.org/10.1016/j.commatsci.2019.109080>

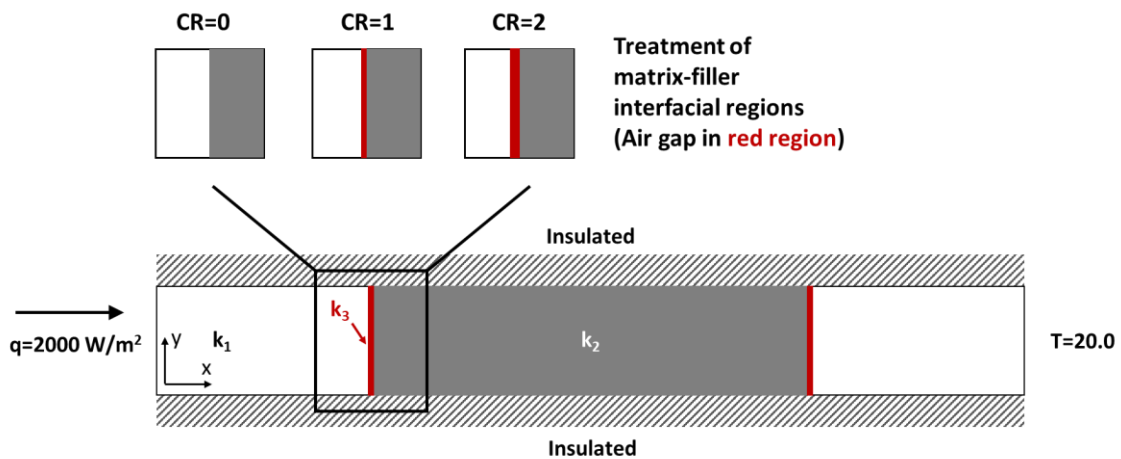
539

540 4.2 Thermal conduction between the filler and matrix interfaces

541 In this section, the thermal conduction between the filler and matrix interfaces in
542 composite material with/without the presence of contact resistance is studied. When
543 simulating the effect of contact resistance in composite materials, it is often practical
544 to use one or two lattices to represent the interfacial region [7], without having to
545 reflect the actual geometry of the rough interfaces. This suggests that instead of using
546 the thermal conductivity of air at the interfacial region, the ETC at the near interfacial
547 region (matrix-gap-filler) should be used. Since the interfacial contact resistance is
548 affected by various properties of the materials used, such as surface roughness,
549 particle sizes and geometries [53], the ETC value of the interfacial region can be
550 estimated either by either using theoretical ETC models [22, 45] or fitting of
551 experimental data [7].

552 However in this study, for the purpose of demonstrating the capability of this
553 SVRP-LBM solver to reflect the interfacial contact resistance, a simplified 2-D
554 geometry shown in Figure 16 is used, and the interfacial region is considered to be
555 filled with dry air. Three different types of interfacial treatments are studied, the
556 geometry CR=0 represents the perfect contact between filler and matrix interfaces,
557 while geometry CR=1 and CR=2 represent the scenarios of different contact
558 resistances due to the imperfect contact between the filler and matrix interfaces. The
559 comparison of temperature profiles at steady states between these three geometries
560 will be able to demonstrate the ability of this SVRP-LBM code to take into account
561 the effect of interfacial contact resistance where applicable.

562



563

564 Figure 16 Schematic diagram of a 2-D geometry for study the effects of interfacial
565 contact resistance at the matrix-filler interfaces. Three different interfacial geometries
566 are used, replacing 0 (CR=0), 1 (CR=1) and 2 (CR=2) lattices at the matrix-filler
567 interfaces with air, where $k_1 = 0.2 \text{ W/m}\cdot\text{K}$ (thermal conductivity of artificial matrix),
568 $k_2 = 20 \text{ W/m}\cdot\text{K}$ (thermal conductivity of artificial filler) and $k_3 = 0.026 \text{ W/m}\cdot\text{K}$ (thermal

Citation:

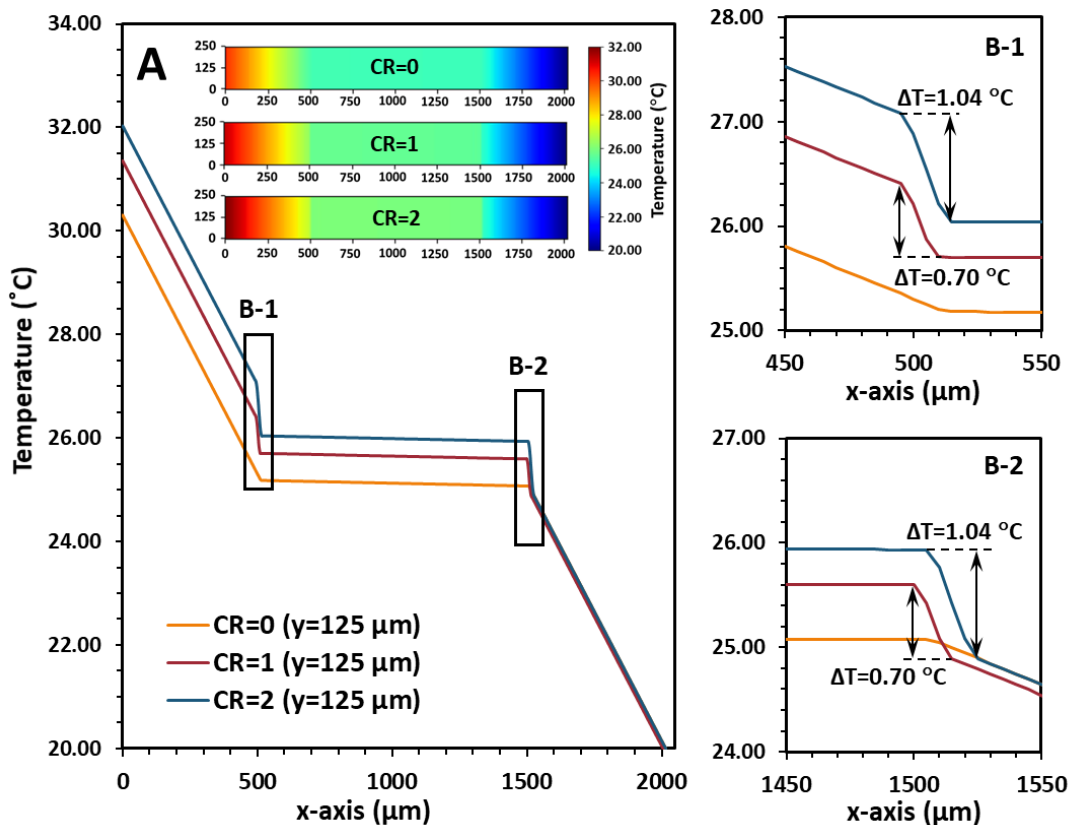
Ke, X.; Duan, Y., A spatially-varying relaxation parameter Lattice Boltzmann Method (SVRP-LBM) for predicting the effective thermal conductivity of composite material. 2019, 169, 109080. <https://doi.org/10.1016/j.commatsci.2019.109080>

569 conductivity of dry air at 25 °C). The LBM lattice number of 404x50 is used for
570 CR=0 and CR=2, while lattice number of 402x50 is used for CR=1.

571

572 The predicted ETC values of geometry CR=0, CR=1 and CR=2 are 0.39 W/m·K,
573 0.36 W/m·K, 0.34 W/m·K respectively, consistent with experimental observations
574 where higher contact resistance resulted in lower thermal conductivities [36, 53, 54].
575 Figure 17 shows the temperature profiles of these three geometries at steady state
576 along the heat flux direction. Among these three geometries, the temperature
577 gradients within the same material (matrix or filler) are the same at steady state,
578 following the Fourier’s law for heat conduction. However, across the entire lattice
579 domain, the temperature differences between the heat source and the isothermal side
580 are higher in geometry CR=1 and CR=2 than CR=0. This is primarily due to the
581 significant temperature drop in the air-filled region. Figure 17B-1 and Figure 17B-2
582 show more detailed comparison of the multi-phases regions between the filler-matrix
583 interfaces. The simulation results show a larger temperature drop in geometry CR=2
584 than geometry CR=1 due to the wider air gap, reflecting a higher contact resistance.

585



586

587 Figure 17 Temperature profiles of geometry CR=0, CR=1 and CR=2 at steady state
588 along the heat flux direction. (A) Horizontally cross the entire geometry; and selected
589 regions (B-1) from 150 μm to 550 μm; (B-2) from 1450 μm to 1550 μm.

590

Citation:

Ke, X.; Duan, Y., A spatially-varying relaxation parameter Lattice Boltzmann Method (SVRP-LBM) for predicting the effective thermal conductivity of composite material. 2019, 169, 109080.
<https://doi.org/10.1016/j.commatsci.2019.109080>

591 For the experimentally prepared composite materials, a larger air gap in between
592 the matrix-filler interfaces can be caused by higher surface roughness. The absolute
593 temperature drop at the matrix-to-filler (Figure 17B-1) and the filler-to-matrix (Figure
594 17B-2) interfaces are the same. This is because the three geometries described in
595 Figure 16 are isotropic in the y-axis direction. At the interfacial region, the heat flux
596 flow along the x-axis direction from the matrix-to-filler and from filler-to-matrix are
597 the same. However, in the case of actual composite materials, the geometries can be
598 much more complex with non-isotropic local microstructures. The heat flux entering
599 and leaving the filler particle might not be the same, leading to different temperature
600 differences [33]. The results shown in Figure 17 prove that this SVRP-LBM solver
601 has the ability to reflect the effect of interfacial contact resistance in composite
602 materials, although geometry configurations need to be considered according to
603 different materials.

604

605 4.3 ETCs of real composite material

606 Before further discussion, we would like to highlight here that the experimental
607 data used in this section for case studies were measured using the guarded hot plate
608 method according to ASTM D5470-17 [55]. This method measures the ETC via
609 monitoring the temperature changes through a thin layer of the composite materials,
610 which is suitable to be simulated via a 2D geometry [22]. The accuracy of this
611 experimental method is about $\pm 2\%$ when the thermal conductivity of the measured
612 material is above 0.1 W/mK [47].

613 Figure 18 compares the measured ETC [25] and LBM predictions of solder
614 composite reinforced by copper spheres at different filler volume fractions. The
615 thermal physical properties of the matrix and the fillers are listed in Table 1. The
616 random composite microstructure is again simulated using the RDFG method. The
617 average filler diameter matches with the actual experimental value (500 μm). No filler
618 size variation is applied according to [25]. Different numbers of fillers are included in
619 the lattice domain in order to simulate filler volume fractions varying from 0.016 to
620 0.296. As shown in Figure 18, the LBM predicted ETC agrees well with the
621 measurements, as well as the theoretical predictions using the Maxwell-Eucken model.
622 It suggests that the LBM algorithm developed in this study can accurately predict the
623 ETC of real composite material reinforced by well-dispersed sphere fillers.

624

625

626

627

628

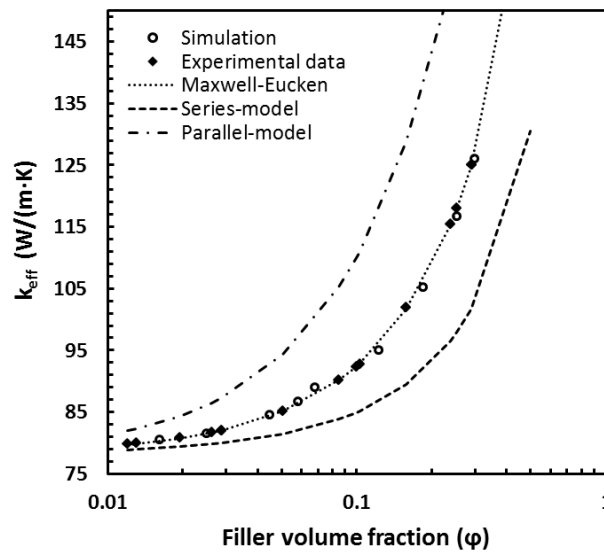
Citation:

Ke, X.; Duan, Y., A spatially-varying relaxation parameter Lattice Boltzmann Method (SVRP-LBM) for predicting the effective thermal conductivity of composite material. 2019, 169, 109080.
<https://doi.org/10.1016/j.commatsci.2019.109080>

629 Table 1 Thermophysical properties of materials chosen for case studies.

	Thermal diffusivity coefficient D (m ² /s)	Thermal conductivity K (W/(m·K))	Density ρ (kg/m ³)	Specific thermal capacity Cp (J/(kg·K))	Ref
Copper	116.00×10 ⁻⁶	398.00	8940	384	[25]
Solder	34.80×10 ⁻⁶	78.10	7360	305	[25]
Silicon rubber	0.10×10 ⁻⁶	0.15	980	1590	[6]
Al ₂ O ₃	8.74×10 ⁻⁶	30.00	3900	880	[6]

630



631

632 Figure 18 Comparison between experimental data and LBM predicted values of
 633 solder composite reinforced with copper spheres [25].

634

635 Figure 19 shows the measured ETC of silicon rubber reinforced by Al₂O₃ fillers of
 636 four different particle sizes sourced from the experimental data shown in [6, 12], and
 637 the corresponded LBM results using either spherical or elliptical fillers. The
 638 calculation using different empirical models are presented in the figure. The thermal
 639 physical properties used for simulations can also be found in Table 1. The mean
 640 diameter sizes of both spherical and elliptical fillers are set as equal to the mean
 641 particle size reported in [6, 12] (d=75 μm, 35 μm, 10 μm or 3 μm). A relative standard
 642 deviation (σ/ξ) of 0.1 is applied to all LBM cases to reflect the filler size variation, as
 643 approximated from particle size distribution reported in the literature [6]. The aspect
 644 ratio of the elliptic filler is fixed as 3:1.

645 As illustrated in the Figure 19 (A-C), when the average filler sizes are larger than
 646 10 μm and the filler volume fraction is higher than 0.1, both the Maxwell-Eucken
 647 model and the LBM model with spherical filler under-predict the ETC. Moreover, the

Citation:

Ke, X.; Duan, Y., A spatially-varying relaxation parameter Lattice Boltzmann Method (SVRP-LBM) for predicting the effective thermal conductivity of composite material. 2019, 169, 109080.
<https://doi.org/10.1016/j.commatsci.2019.109080>

648 predicted ETC using spherical fillers follows the Maxwell-Eucken prediction at lower
649 filler volume fraction (<0.2), while at higher filler volume fraction, the LBM
650 predictions using spherical fillers are slightly higher than the Maxwell-Eucken
651 prediction. The same phenomenon has been observed from the mass diffusion process
652 in porous media, where the LBM prediction is always higher than the Maxwell-
653 Eucken model prediction in high porosity media [56]. The positive contribution of the
654 particle size variation as discussed in section 4.1 may be one of the reasons.

655 When using ellipses fillers with an aspect ratio of 3:1, positioned parallel to the
656 heat flux direction, the predicted ETC using the elliptical fillers showed good
657 agreement with the experimental results when the average filler sizes are above 10 μm .
658 The scanning electron microscope (SEM) images of the Al_2O_3 filler particles used for
659 preparing this composite material showed plate-shaped geometry [12, 57]. The shape-
660 effect of the filler, as discussed in the previous section, might explain the good
661 performance of the LBM model with ellipses filler, which might also explain the
662 under-prediction of the Maxwell-Eucken model and the LBM model with spherical
663 filler.

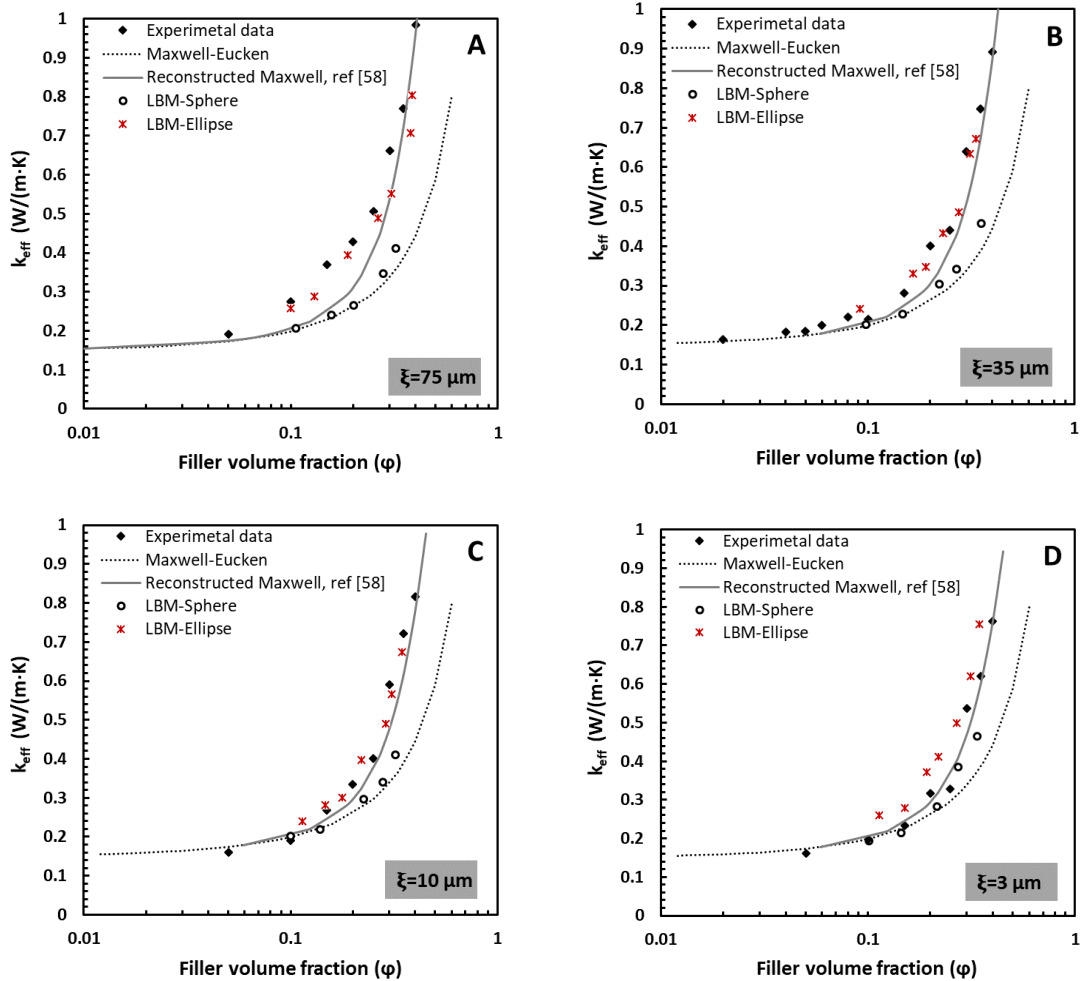
664 Additionally, Xu et al [58] proposed a reconstructed Maxwell-Eucken model to fit
665 the experimental data, contributing the higher ETC to the contact resistance between
666 the particles. The reconstructed model fitted to these experimental data has also been
667 plotted in Figure 19. In comparison with the reconstructed Maxwell-Eucken model,
668 the LBM prediction using elliptical fillers also shows better agreement with
669 experimental data (for filler size above 10 μm). The reconstructed model proposed by
670 Xu et al. [58] is based on the assumption that every two particles will be connected
671 together (with additional contact resistance between the two particles), which shares
672 some similarities with the elliptical fillers.

673 In the cases of the smallest filler ($\xi=3 \mu\text{m}$ Figure 19D), the LBM model with
674 elliptical fillers leads to over-prediction of ETC; while the use of spherical fillers
675 results in closer predictions. For commonly used non-spherical filler particles, such as
676 Al_2O_3 , ZnO, TiB_2 , SiC and talc, the same material with very small particle sizes often
677 possess the sphere-like feature [12, 43, 57], while larger particles often possess the
678 non-spherical feature This is similar to that has been observed from carbon nanotube
679 (CNT) reinforced composite, where larger CNT showed higher aspect ratio and led to
680 higher ETC [59, 60]. This further supports the assumptions that the geometry effect
681 could be one of the main factors that led to the greater enhanced ETCs of larger Al_2O_3
682 particles reinforced composite materials at high filler volume fraction.

683

Citation:

Ke, X.; Duan, Y., A spatially-varying relaxation parameter Lattice Boltzmann Method (SVRP-LBM) for predicting the effective thermal conductivity of composite material. 2019, 169, 109080. <https://doi.org/10.1016/j.commatsci.2019.109080>



684

685

686 Figure 19 Experimental data, LBM prediction and empirical model output of ETCs of
687 silicon rubber reinforced with Al₂O₃ fillers [6, 12].

688

689 **5 Conclusion**

690 The in-house coded spatially-varying relaxation parameter Lattice Boltzmann
691 Method (SVRP-LBM) solver has been validated for predicting the effective thermal
692 conductivity (ETC) of various composite materials, including simulating the
693 interfacial contact resistance. It is found that higher prediction accuracy can be
694 achieved when the lowest chosen relaxation parameter approaches 1.0, for composite
695 materials with large thermal diffusivity ratios. The predictions also showed good
696 agreement with experiments data when choosing the right representative filler
697 geometries.

698 The effects of filler geometry (orientation and shape) and filler size variation on
699 the thermal conduction behaviour of simulated composite material are assessed using
700 SVRP-LBM solver. The predicted ETC increases as the filler volume fraction

Citation:

Ke, X.; Duan, Y., A spatially-varying relaxation parameter Lattice Boltzmann Method (SVRP-LBM) for predicting the effective thermal conductivity of composite material. 2019, 169, 109080.
<https://doi.org/10.1016/j.commatsci.2019.109080>

701 increases. At the same filler volume fraction, the elliptical fillers parallel to the heat
702 flow direction achieved the highest ETC, possibly attributed by the enhanced thermal
703 conduction path along the heat flux direction. Higher filler size variance can result in
704 higher ETC, likely due to the improved filler packing efficiency.

705 The SVRP-LBM solver developed in this study can be used to design filler
706 reinforced composite material with targeted ETC and local temperature distribution
707 requirement. As the initial development of a predictive design tool for functional
708 composite materials, an extension of this method to the three-dimensional solver and
709 quantification of uncertainties brought by the random location effect will further
710 improve the accuracy of this model, which will be discussed in future studies.

711

712 Acknowledgement

713 The participation of XK was sponsored by University of Bath Prize Fellowship.

714 Data Availability

715 The raw and processed data required to reproduce these findings cannot be shared at
716 this time as the data also forms part of an ongoing study.

717 References

- 718 1. Mamunya, Y.P., et al., *Electrical and thermal conductivity of polymers filled*
719 *with metal powders*. European Polymer Journal, 2002. **38**(9): p. 1887-1897.
- 720 2. Fu, Y.-X., et al., *Thermal conductivity enhancement of epoxy adhesive using*
721 *graphene sheets as additives*. International Journal of Thermal Sciences, 2014.
722 **86**: p. 276-283.
- 723 3. Tong, X.C., *Advanced Materials for Thermal Management of Electronic*
724 *Packaging*. Vol. 30. 2011: Springer-Verlag New York. 618.
- 725 4. Agyenim, F., et al., *A review of materials, heat transfer and phase change*
726 *problem formulation for latent heat thermal energy storage systems (LHTESS)*.
727 *Renewable and Sustainable Energy Reviews*, 2010. **14**(2): p. 615-628.
- 728 5. Mukherjee, P.P., Q. Kang, and C.-Y. Wang, *Pore-scale modeling of two-phase*
729 *transport in polymer electrolyte fuel cells—progress and perspective*. Energy
730 & Environmental Science, 2011. **4**(2): p. 346-369.
- 731 6. Gao, B.Z., et al., *Experimental and theoretical studies of effective thermal*
732 *conductivity of composites made of silicone rubber and Al₂O₃ particles*.
733 *Thermochimica Acta*, 2015. **614**: p. 1-8.
- 734 7. Li, L., et al., *Study on effective thermal conductivity of silicone/phosphor*
735 *composite and its size effect by Lattice Boltzmann method*. Heat and Mass
736 Transfer, 2016. **52**(12): p. 2813-2821.
- 737 8. Sengul, O., et al., *Effect of expanded perlite on the mechanical properties and*
738 *thermal conductivity of lightweight concrete*. Energy and Buildings, 2011.
739 **43**(2): p. 671-676.

Citation:

Ke, X.; Duan, Y., A spatially-varying relaxation parameter Lattice Boltzmann Method (SVRP-LBM) for predicting the effective thermal conductivity of composite material. 2019, 169, 109080.
<https://doi.org/10.1016/j.commatsci.2019.109080>

- 740 9. Cahill, D.G., et al., *Nanoscale thermal transport*. Journal of Applied Physics,
741 2003. **93**(2): p. 793-818.
- 742 10. Burger, N., et al., *Review of thermal conductivity in composites: Mechanisms,*
743 *parameters and theory*. Progress in Polymer Science, 2016. **61**: p. 1-28.
- 744 11. Hussain, A.R.J., et al., *Review of polymers for heat exchanger applications:*
745 *Factors concerning thermal conductivity*. Applied Thermal Engineering, 2017.
746 **113**: p. 1118-1127.
- 747 12. Sim, L.C., et al., *Thermal characterization of Al₂O₃ and ZnO reinforced*
748 *silicone rubber as thermal pads for heat dissipation purposes*. Thermochemica
749 Acta, 2005. **430**(1): p. 155-165.
- 750 13. Fu, Y.-X., et al., *Thermal conductivity enhancement with different fillers for*
751 *epoxy resin adhesives*. Applied Thermal Engineering, 2014. **66**(1): p. 493-498.
- 752 14. Zhai, S., et al., *Effective thermal conductivity of polymer composites:*
753 *Theoretical models and simulation models*. International Journal of Heat and
754 Mass Transfer, 2018. **117**: p. 358-374.
- 755 15. Tekce, H.S., D. Kumlutas, and I.H. Tavman, *Effect of Particle Shape on*
756 *Thermal Conductivity of Copper Reinforced Polymer Composites*. Journal of
757 Reinforced Plastics and Composites, 2007. **26**(1): p. 113-121.
- 758 16. Chen, H., et al., *Thermal conductivity of polymer-based composites:*
759 *Fundamentals and applications*. Progress in Polymer Science, 2016. **59**: p. 41-
760 85.
- 761 17. Benveniste, Y., *Effective thermal conductivity of composites with a thermal*
762 *contact resistance between the constituents: Nondilute case*. Journal of
763 Applied Physics, 1987. **61**(8): p. 2840-2843.
- 764 18. Mori, T. and K. Tanaka, *Average stress in matrix and average elastic energy*
765 *of materials with misfitting inclusions*. Acta Metallurgica, 1973. **21**(5): p. 571-
766 574.
- 767 19. Azadi, P., R. Farnood, and N. Yan, *FEM-DEM modeling of thermal*
768 *conductivity of porous pigmented coatings*. Computational Materials Science,
769 2010. **49**(2): p. 392-399.
- 770 20. Duan, Y., et al., *Analysis of the horizontal flow in the advanced gas-cooled*
771 *reactor*. Nuclear Engineering and Design, 2014. **272**: p. 53-64.
- 772 21. Wang, M., et al., *Mesosopic predictions of the effective thermal conductivity*
773 *for microscale random porous media*. Physical Review E, 2007. **75**(3): p.
774 036702.
- 775 22. Zhou, F. and G. Cheng, *Lattice Boltzmann model for predicting effective*
776 *thermal conductivity of composite with randomly distributed particles:*
777 *Considering effect of interactions between particles and matrix*.
778 Computational Materials Science, 2014. **92**: p. 157-165.
- 779 23. Walther, E., R. Bennacer, and C. De Sa, *Lattice Boltzmann Method and*
780 *diffusion in materials with large diffusivity ratios*. Thermal science, 2017.
781 **21**(3): p. 1173-1182.
- 782 24. Cao, A. and J. Qu, *Size dependent thermal conductivity of single-walled*
783 *carbon nanotubes*. Journal of Applied Physics, 2012. **112**(1): p. 013503.
- 784 25. Lee, H.J. and R.E. Taylor, *Thermal diffusivity of dispersed composites*. Journal
785 of Applied Physics, 1976. **47**(1): p. 148-151.
- 786 26. Sanada, K., Y. Tada, and Y. Shindo, *Thermal conductivity of polymer*
787 *composites with close-packed structure of nano and micro fillers*. Composites
788 Part A: Applied Science and Manufacturing, 2009. **40**(6): p. 724-730.

Citation:

Ke, X.; Duan, Y., A spatially-varying relaxation parameter Lattice Boltzmann Method (SVRP-LBM) for predicting the effective thermal conductivity of composite material. 2019, 169, 109080.
<https://doi.org/10.1016/j.commatsci.2019.109080>

- 789 27. Wang, M. and N. Pan, *Modeling and prediction of the effective thermal*
790 *conductivity of random open-cell porous foams*. International Journal of Heat
791 and Mass Transfer, 2008. **51**(5): p. 1325-1331.
- 792 28. Lu, J.H., H.Y. Lei, and C.S. Dai, *A lattice Boltzmann algorithm for simulating*
793 *conjugate heat transfer through virtual heat capacity correction*. International
794 Journal of Thermal Sciences, 2017. **116**: p. 22-31.
- 795 29. Fang, W.-Z., et al., *Predictions of effective thermal conductivities for three-*
796 *dimensional four-directional braided composites using the lattice Boltzmann*
797 *method*. International Journal of Heat and Mass Transfer, 2016. **92**: p. 120-130.
- 798 30. Krüger, T., et al., *The Lattice Boltzmann Method: Principles and Practice*.
799 2016: Springer International Publishing.
- 800 31. Wang, J., M. Wang, and Z. Li, *A lattice Boltzmann algorithm for fluid–solid*
801 *conjugate heat transfer*. International Journal of Thermal Sciences, 2007.
802 **46**(3): p. 228-234.
- 803 32. Evans, W., et al., *Effect of aggregation and interfacial thermal resistance on*
804 *thermal conductivity of nanocomposites and colloidal nanofluids*. International
805 Journal of Heat and Mass Transfer, 2008. **51**(5-6): p. 1431-1438.
- 806 33. Deng, Z., et al., *Heat Conduction in Porous Media Characterized by Fractal*
807 *Geometry*. Energies, 2017. **10**(8): p. 1230.
- 808 34. Pollack, G.L., *Kapitza Resistance*. Reviews of Modern Physics, 1969. **41**(1): p.
809 48-81.
- 810 35. Nan, C.-W., et al., *Interface effect on thermal conductivity of carbon nanotube*
811 *composites*. Applied Physics Letters, 2004. **85**(16): p. 3549-3551.
- 812 36. Gharagozloo-Hubmann, K., et al., *Filler geometry and interface resistance of*
813 *carbon nanofibres: Key parameters in thermally conductive polymer*
814 *composites*. Applied Physics Letters, 2013. **102**(21): p. 213103.
- 815 37. Wang, Z.L., et al., *Thermal boundary resistance and temperature dependent*
816 *phonon conduction in CNT array multilayer structure*. International Journal of
817 Thermal Sciences, 2013. **74**: p. 53-62.
- 818 38. Mohamad, A., *Lattice Boltzmann Method Fundamentals and Engineering*
819 *Applications with Computer Codes*. 2011.
- 820 39. Bhatnagar, P.L., E.P. Gross, and M. Krook, *A Model for Collision Processes*
821 *in Gases. I. Small Amplitude Processes in Charged and Neutral One-*
822 *Component Systems*. Physical Review, 1954. **94**(3): p. 511-525.
- 823 40. Zou, Q. and X. He, *On pressure and velocity boundary conditions for the*
824 *lattice Boltzmann BGK model*. Physics of Fluids, 1997. **9**(6): p. 1591-1598.
- 825 41. Zain-ul-abdein, M., et al., *Numerical investigation of the effect of interfacial*
826 *thermal resistance upon the thermal conductivity of copper/diamond*
827 *composites*. Materials & Design, 2015. **86**: p. 248-258.
- 828 42. Kim, C.P., et al., *Processing of carbon-fiber-reinforced*
829 *Zr_{41.2}Ti_{13.8}Cu_{12.5}Ni_{10.0}Be_{22.5} bulk metallic glass composites*. Applied
830 Physics Letters, 2001. **79**(10): p. 1456-1458.
- 831 43. Guise, O., C. Strom, and N. Preschilla, *STEM-in-SEM method for morphology*
832 *analysis of polymer systems*. Polymer, 2011. **52**(5): p. 1278-1285.
- 833 44. Shakoor, A. and N.L. Thomas, *Talc as a nucleating agent and reinforcing*
834 *filler in poly(lactic acid) composites*. Polymer Engineering & Science, 2014.
835 **54**(1): p. 64-70.
- 836 45. Mohamad, A.A., et al., *Treatment of Transport at the Interface Between*
837 *Multilayers via the Lattice Boltzmann Method*. Numerical Heat Transfer, Part
838 B: Fundamentals, 2015. **67**(2): p. 124-134.

Citation:

Ke, X.; Duan, Y., A spatially-varying relaxation parameter Lattice Boltzmann Method (SVRP-LBM) for predicting the effective thermal conductivity of composite material. 2019, 169, 109080.
<https://doi.org/10.1016/j.commat.2019.109080>

- 839 46. Maxwell, J.C., *A treatise on electricity and magnetism*. 1881: Clarendon Press.
- 840 47. Hammerschmidt, U., *Guarded Hot-Plate (GHP) Method: Uncertainty*
841 *Assessment*. International Journal of Thermophysics, 2002. **23**(6): p. 1551-
842 1570.
- 843 48. Deissler, R.G. and J.S. Boegli, *An investigation of effective thermal*
844 *conductivities of powders in various gases*. Trans. Am. Soc. Mech. Engrs.,
845 1958: p. Medium: X; Size: Pages: 1417-25.
- 846 49. Xu, Y. and K. Yagi, *Automatic FEM model generation for evaluating thermal*
847 *conductivity of composite with random materials arrangement*. Computational
848 Materials Science, 2004. **30**(3): p. 242-250.
- 849 50. Mu, Q., S. Feng, and G. Diao, *Thermal conductivity of silicone rubber filled*
850 *with ZnO*. Polymer Composites, 2007. **28**(2): p. 125-130.
- 851 51. Nan, C.-W., et al., *Effective thermal conductivity of particulate composites*
852 *with interfacial thermal resistance*. Journal of Applied Physics, 1997. **81**(10):
853 p. 6692-6699.
- 854 52. Choi, S. and J. Kim, *Thermal conductivity of epoxy composites with a binary-*
855 *particle system of aluminum oxide and aluminum nitride fillers*. Composites
856 Part B: Engineering, 2013. **51**: p. 140-147.
- 857 53. Zhang, P., Q. Li, and Y. Xuan, *Thermal contact resistance of epoxy*
858 *composites incorporated with nano-copper particles and the multi-walled*
859 *carbon nanotubes*. Composites Part A: Applied Science and Manufacturing,
860 2014. **57**: p. 1-7.
- 861 54. Sadeghi, E., S. Hsieh, and M. Bahrami, *Thermal conductivity and contact*
862 *resistance of metal foams*. Journal of Physics D: Applied Physics, 2011.
863 **44**(12): p. 125406.
- 864 55. ASTM, *D5470-17*, in *Standard Test Method for Thermal Transmission*
865 *Properties of Thermally Conductive Electrical Insulation Materials*. 2017,
866 ASTM International: West Conshohocken, PA.
- 867 56. Xuan, Y.M., K. Zhao, and Q. Li, *Investigation on mass diffusion process in*
868 *porous media based on Lattice Boltzmann method*. Heat and Mass Transfer,
869 2010. **46**(10): p. 1039-1051.
- 870 57. Hill, R.F. and P.H. Supancic, *Thermal Conductivity of Platelet-Filled Polymer*
871 *Composites*. Journal of the American Ceramic Society, 2002. **85**(4): p. 851-
872 857.
- 873 58. Xu, J.Z., B.Z. Gao, and F.Y. Kang, *A reconstruction of Maxwell model for*
874 *effective thermal conductivity of composite materials*. Applied Thermal
875 Engineering, 2016. **102**: p. 972-979.
- 876 59. Deng, F., et al., *Effects of anisotropy, aspect ratio, and nonstraightness of*
877 *carbon nanotubes on thermal conductivity of carbon nanotube composites*.
878 Applied Physics Letters, 2007. **90**(2): p. 021914.
- 879 60. Li, J., et al., *Correlations between Percolation Threshold, Dispersion State,*
880 *and Aspect Ratio of Carbon Nanotubes*. Advanced Functional Materials, 2007.
881 **17**(16): p. 3207-3215.

882